JPRS-JST-90-006
2 FEBRUARY 1990

FOREIGN BROADCAST INFORMATION SERVICE

JPRS Report

Science & Technology

Japan

3RD FUNCTIONALLY GRADIENT MATERIALS SYMPOSIUM

JPRS-JST-90-006
2 FEBRUARY 1990

SCIENCE & TECHNOLOGY

JAPAN

3RD FUNCTIONALLY GRADIENT MATERIALS SYMPOSIUM

[Selections from the 3rd Functionally Gradient Materials Symposium held 14 Sep 89 in Tokyo, sponsored by the Functionally Gradient Materials Forum]

43067008 Tokyo FGM 89 in Japanese 14 Sep 89 pp v-viii, 1-172

CONTENTS

Program

43067008A Tokyo FGM 89 in Japanese 14 Sep 89 pp v-viii

[Text] (Synthesis)

Wide-Area Control Technology for Functionally Gradient Materials by the SHS (Self-Propagating High-Temperature Synthesis) Process and Various Properties of TiB_2-Cu Materials

43067008B Tokyo FGM 89 in Japanese 14 Sep 89 pp 23-26

[Report by Nobuhiro Sata, Norio Yanagisawa, Kazuyuki Nagata, Osamu Asano and Norio Sanada of GIRI, Tohoku]

[Text] 1. Introduction

Research and development of functionally gradient materials by the self-propagating high-temperature synthesizing process (SHS method) are being pursued, particularly as regards their expansion to the 30-cm square level in the future (target for the second-term coordination expenditures for the promotion of science and technology).[1-6] Here we will focus on wide-area control techniques as an important practical means in the creation of functionally gradient materials as well as on the results of measuring various properties of materials based on the TiB_2-Cu system, which are currently a subject for research on the synthesis of functionally gradient materials.

Solid-state powder is basically used as the raw material of functionally gradient materials to be produced by the SFS method that is currently under study. Therefore, to cause the composition of a material, unevenly inclined as in the case of functionally gradient materials, to be distributed according to a design, it is necessary to adopt a technology to laminate it while changing the mixed composition of the material powder by the same process as powder metallurgy. Also, in order to form in high density during the synthesis, it is necessary to use a simultaneous synthesis and formation technology by applying pressure at the same time. Figure 1 shows a series of practical processes to synthesize functionally gradient materials by the SHS method.

2. Automatic Gradient Laminate Control Technique

We are currently tackling the development of automatic laminating and filling up equipment able to synthesize discoidal functionally gradient materials with a 30 mm-level diameter. Figure 2 [not reproduced] shows the external appearance of the equipment, and the specifications for it are outlined below:

1) The spray region is to be scanned with an X-Y stage so that lamination can be achieved uniformly in a wide area.

2) A spray nozzle is to be placed in the upper part of the X-Y stage, thereby spraying and laminating material powders.

3) The raw materials are to be separately supplied to the spray nozzle by a liquid carrying method.

4) Gradiently mixed composition of the material powders, the spray speed, spray patterns and areas are all to be controlled with a PC9800 computer.

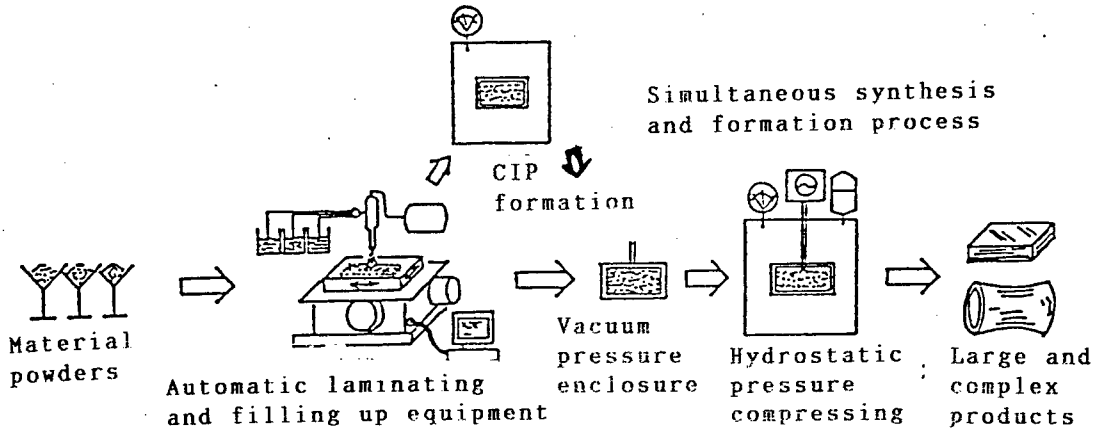

Figure 1. Practical processes to synthesize functionally gradient materials by the SHS method

As a result of our experiments on laminate filling through the use of this equipment, it has become clear that this equipment involves difficulties such as the time for lamination, the spray nozzle and the conveyance of material powders of comparatively large grain. We will make further efforts to focus on and improve these problem points.

We are also checking into a plan to produce large, 30 cm^2 level automatic laminate filling equipment on a practical scale in this fiscal year, bearing these results in mind and also taking the trends toward larger areas, larger capacities and higher speed into consideration.

3. Hydrostatic Pressure Applied Synthesis Technology

Figure 3 shows simultaneous synthesis and forming equipment using hydrostatic pressure, currently adopted by the GIRI, Tohoku.

The basic structure of this equipment should be called an advanced CIP (cold isotropic pressurizer) equipped with an accumulator for pressure compensation and an electrode for ignition purposes. It is expected to be used in the future as a powerful means of creating functionally gradient materials by the SHS method. Some characteristics of the hydrostatic pressure method are itemized below:

1) The pressure time is short because water is used as the pressure medium. Also, the reduction of pressure is rapid because water has high compressibility. Therefore, this method involves less danger.

2) Since the equipment is used at normal temperature, a heating source is not necessary, making it easy to increase its size as pressure equipment.

3) An accumulator is connected and used to cope with a drop in pressure due to such factors as the shrinkage of test samples during synthesis.

4) Water acts as an agent to diffuse or absorb the heat generated during synthesis. The cooling speed of the sample should be adjusted by placing an adiabatic layer appropriately. It is also possible to control temperature (by the chemical oven method) in such a way as to raise the environmental temperature by placing a reactive material around the sample as a heating source.

5) Use of an ignition method called a fine wire induction arc method will make it possible to easily synthesize and form independent, multiple samples in one pressure vessel. It is also possible to synthesize and form multiple samples in one hermetical vessel by providing a graphite sheet partition.

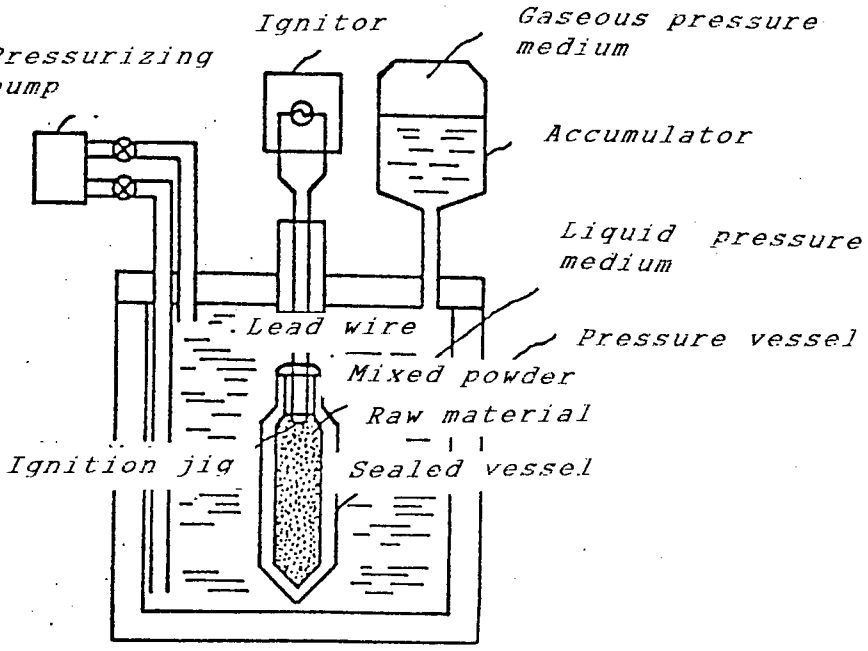

Figure 3. Typical example of hydrostatic pressure applied synthesis equipment

We introduced new experimental equipment in fiscal 1988. The pressurizing force is a maximum of 60 MPa and the inner capacity is 120 mm ϕ x 250 mmh. We are checking into synthesizing a 10 cm square FGM in the near future. This equipment is equipped with a window whereby synthetic reactions can be

observed in high-pressure water. We are also observing the situation in which actual reactions are taking place.

4. Thermal and Mechanical Properties of TiB_2-Cu Non-Gradient Materials

The thermal expansion rate is shown in Figure 5, the thermal diffusion rate in Figure 6, the specific heat in Figure 7, the thermal conductivity in Figure 8, the density in Figure 9 and Young's modulus in Figure 10. The thermal diffusion rate and the specific heat measured 4 under the laser flush method, and the thermal conductivity was sought from these values and the density. Young's modulus was sought through SP and MSP tests and through bending tests. Together with these basic property values, we intend to report our measurements of the characteristic values of composition containing Cu by more than 60 wt% and also the evaluation of the bending strength, SP energy, porocity, high-temperature oxidation properties, etc.

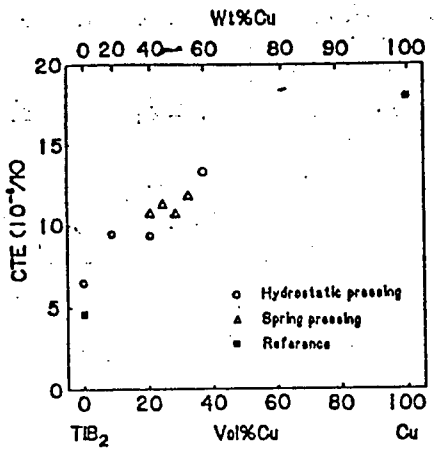

Figure 5. Thermal expansion rate

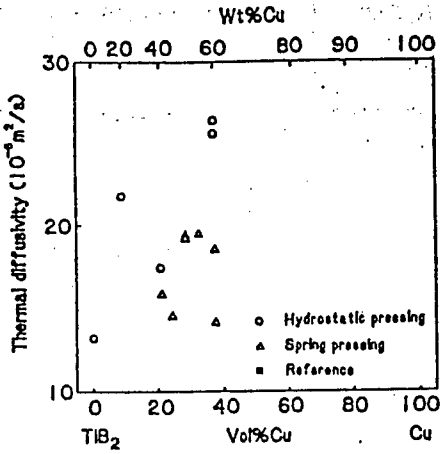

Figure 6. Thermal diffusion rate

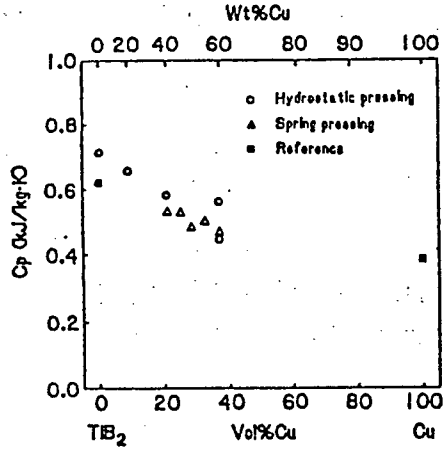

Figure 7. Specific heat

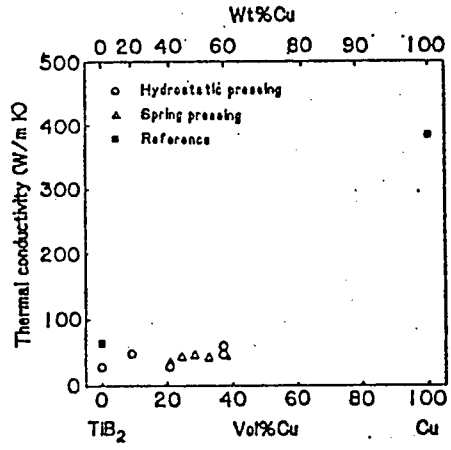

Figure 8. Thermal conductivity

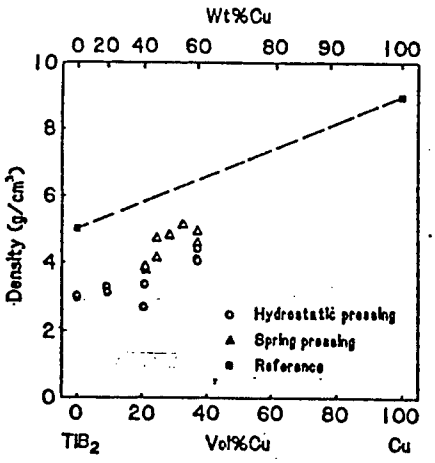

Figure 9. Density

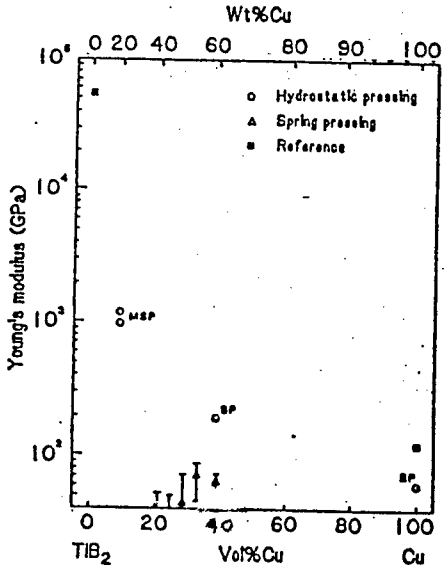

Figure 10. Young's modulus

5. Conclusion

As for the synthesis of TiB_2-Cu system gradient materials by the SHS method, it is possible to synthesize 30 mm ϕ-level materials. On the basis of the information obtained so far, we will tackle the task of improving surface qualities (including the granting of oxidation resistance to surface ceramic layers), which has been pending, and also study the qualitative improvement of materials for the internal control of thermal properties. In addition, we want to pursue our studies with a view to further expanding the areas of control.

References

1. Sata, Functional Materials, 8, 47-58 (1987).

2. Sata, Industrial Powder, 49, 242-249 (1988).

3. N. Sata, et al., Proc. of MRS Int. Meet. on Advanced Material, Tokyo, June 1988.

4. N. Sata, et al., 1st Int. Symp. on Combustion and Plasma Synthesis of High Temperature Materials, San Francisco, October 1988.

5. Sata, Ceramics, 24 [6] 514-520 (1989).

6. Sata, Metals, 59 [6] 7-13 (1989).

Production of Ni-ZrO_2 Functionally Gradient Materials by the Dispersive Plating Method

43067008C Tokyo FGM 89 in Japanese 14 Sep 89 pp 31-34

[Report by Kiyoshi Kuruma, Masaki Abe, Akihide Yoshitake and Manabu Tamura of the NKK Steel Research Laboratory and Masayuki Niino of the National Aerospace Laboratory]

[Text] 1. Introduction

Attention is being focused on functionally gradient materials as heat-proof materials for next generation aircraft fuselages and engines, characterized by a change in composition to a greater depth. The dispersive plating method, enabling a metal and a nonmetal to be densely compounded to each other, is one of the powerful means of producing functionally gradient materials. Here we will report the result of our attempt at component control of Ni-ZrO_2 dispersive plating and the result of forming a dispersive plated layer on Ni-ZrO_2 ceramics. We will also describe the result of our examination of the strength of plated films.

2. Method of Experiments

The composition of the plating bath and the plating terms are shown in Table 1.

Table 1. Plating Terms

Bath	Sulfamine acid nickel	500	g/l
	Boric acid	30	g/l
Plating terms	Bath temperature	50	°C
	pH	3.5	
	ZrO_2 grain size	1-2	μm
	Current density	1-5	A/dm^2
	ZrO_2 concentration	0-100	g/l

As a substrate we used a thin film ceramic produced by a Ni leaf by the Dr Blade method. The ZrO_2 content in the Ni plated layer was sought by the fluorescent X-ray method, and the depth distribution of the ZrO_2 was measured by SIMS. In addition, the strength of the plated film was measured by the small punch test (hereinafter referred to as the SP test). The theory of the SP test is given in Figure 1.

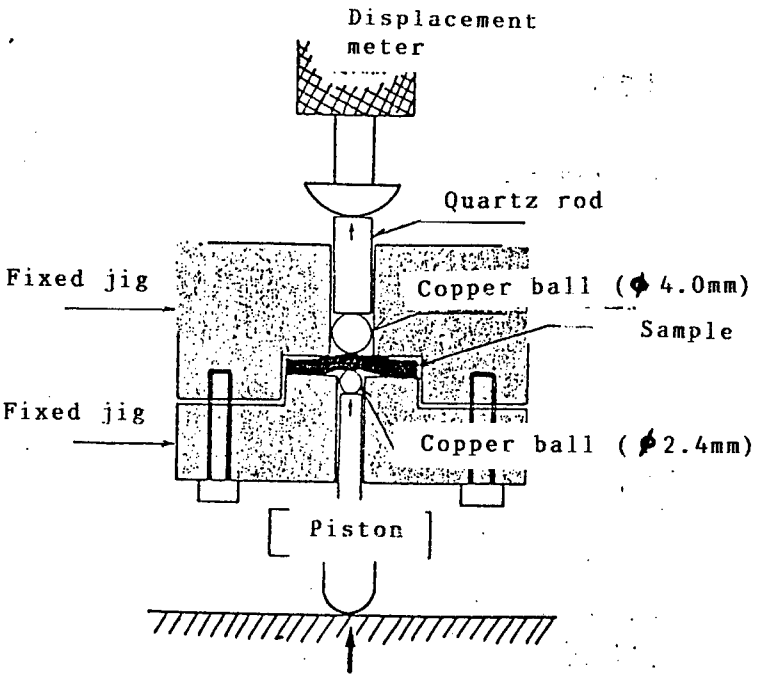

Figure 1. Theory of SP test

3. Result of Experiments

3.1. Plating Terms and ZrO_2 Content in the Plated Layer

Figure 2 shows the relationship between the ZrO_2 concentration in the plating bath and the ZrO_2 content in the plated layer. The illustration shows that the higher the ZrO_2 concentration in the plating bath and the lower the current density, the greater the increase in the amount of ZrO_2 in the plated layer. Within the limits of the experiments conducted this time, the maximum ZrO_2 content is a little less than 30 vol percent.

3.2. Preparation of 2-Gradient Plated Layer

On the basis of Figure 2, we selected appropriate plating terms and prepared a gradient plated layer. A sectional SEM photo of an Ni-ZrO_2 gradient component material, with the ZrO_2 content changed to 0-25vol%, is shown in Figure 3 (a), and its component change in terms of depth is shown in Figure 3 (b). The component gradient is in five stages, and the substrate is made of a 50 μm Ni leaf.

3.3. Dispersive Plating on Thin Film Ceramics

Since it is difficult to form ZrO_2-rich layers by the dispersive plating method, we looked at a combination with ceramics. Figure 4 [not reproduced] is an optical microscopic photo of Ni-ZrO_2 gradient component materials (7 layers in total), with ZrO_2 content changed to the rate of 25-0 vol percent on Ni70 vol%-$ZrO_2$30 vol% thin film ceramics 500 μm thick, produced

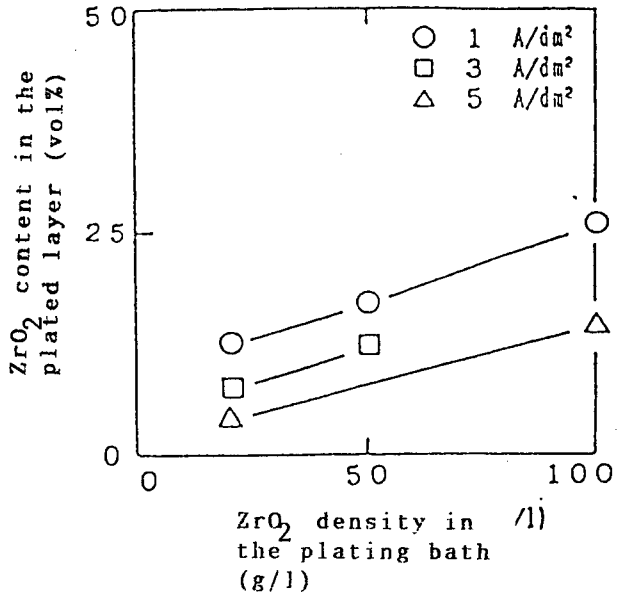

Figure 2. Relationship between the ZrO_2 concentration in the bath and the ZrO_2 content in the plated layer

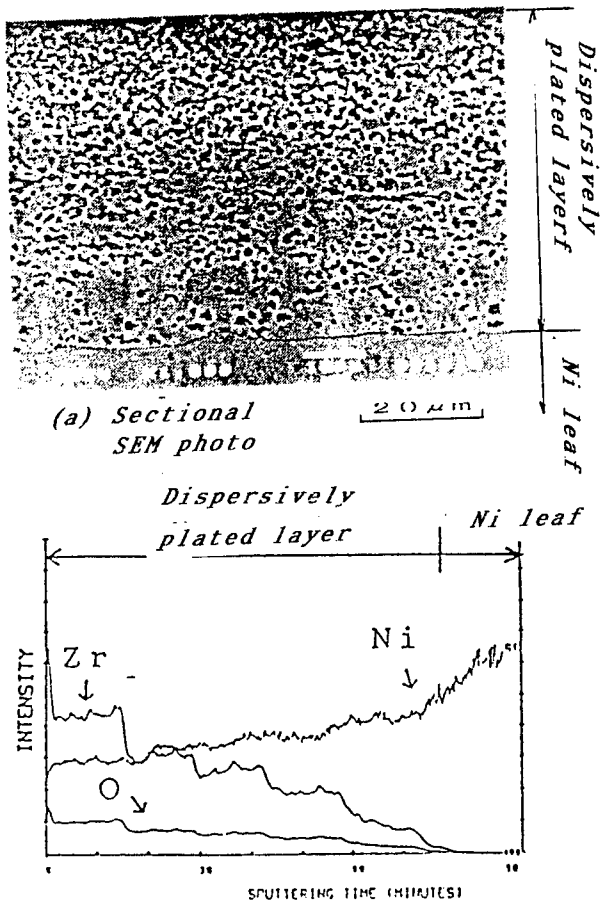

(b) Analysis of depth by SIMS

Figure 3. Gradiently plated layer on metal

by the Dr Blade method. We confirmed that the plating involved a satisfactory junction interface for ceramics as well.

3.4. Strength Evaluation of Ceramics-Dispersive Plating Complex

To examine the strength of a complex with dispersive plated layers piled up on ceramics, we placed Ni single layer plating (100 μm thick), containing 0, 5, 10, 15 and 25 vol% ZrO_2, on Ni70 vol%-$ZrO_2$30 vol% ceramics (substrate), and put them to SP tests. We added a load from the side of the plated layer. As a result, every material was cracked radially on the substrate side, but no crack was seen on the film side. As an example, Figure 5 [not reproduced] shows SEM photos of the outside and inside of a sample used to carry out SP tests on the plating of 10 vol% ZrO_2 containing Ni. From the result of our test on a load-displacement curve, too, we discovered that the transformation of the dispersive plated layer is ductile even in the case of ZrO_2 content up to about 25 vol%. As no exfoliation between the ceramics and the plated layer was seen after the transformation, it is conceivable that the dispersive plated layer can be expected to serve as a means of reinforcing ceramics (preventing the progress of cracking).

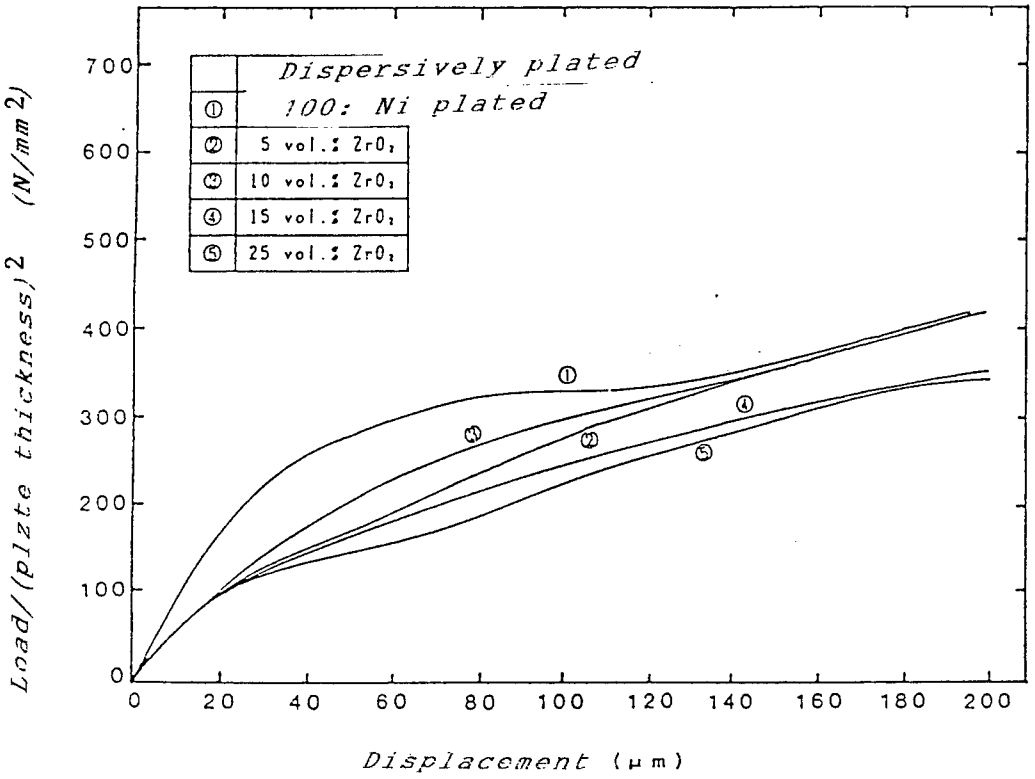

Figure 6. Displacement curves in the case of a load placed on ceramics and dispersive plated composite layer

4. Conclusion

The dispersive plating method makes it possible to adjust the Ni-ZrO_2 component ratio with relative ease by changing the amount of ZrO_2 to be added to the plating bath, current density, etc., and also to form a plated layer on the Ni-ZrO_2 composite ceramics as well. Therefore, we found that it is possible to produce functionally gradient materials with the composition arbitrarily controlled from 0 to 100 percent through a combination of ceramics, the composition of which is changed continuously, and dispersive plating. It was also recognized that a low ZrO_2-high Ni layer formed by the dispersive plating method is effective in preventing the progress of fragile cracks in ceramics during transformation.

This research is part of the result of the "Research on the Basic Technology for the Development of Functionally Gradient Materials To Reduce Thermal Stress," conducted with the Science and Technology Agency's expenditures for the promotion and coordination of science and technology for fiscal 1988. (Partially announced at the 79th speech meeting held by the Surface Technology Association.)

Design and Production of Discoid Functionally Gradient Materials

43067008D Tokyo FGM 89 in Japanese 14 Sep 89 pp 49-54

[Report by Akira Kawasaki, Masahiko Iijima and Ryuzo Watanabe of Tohoku University]

[Text] 1. Introduction

We, the authors, are pursuing research on sintered functionally gradient materials by a particle spray method.[1,2] To produce sound sintered functionally gradient materials, it is necessary to carry out designs taking into consideration such matters as 1) holding down the fluctuation in sintering speed due to composition to a low level, that is, keeping the balance of sintering shrinkage, 2) achieving structural control to ensure strength and tenacity, and 3) easing the thermal stress occurring during production. To date, we have obtained a zirconia/stainless steel gradient composition control layer 8 mm across and 20 mm high and a sound discoid gradient material 4 mm thick by easing the thermal stress through optimum composition control.[3,4] In this case, the stress component to be noted to ease the thermal stress lies in the axial stress arising in the vicinity of the sample surface. However, in the case of size increase aimed at practical use in the future, that is, in the case of producing discoid functionally gradient materials constituting a low height vs diameter rate (hereinafter referred to in terms of h/d), it is not sufficient to grasp the axial stress alone. It is necessary to grasp the stress situation involving thermal stress components as well, such as circumferential stress, radial stress and shearing stress.

In this research we analyzed the thermal stress arising during production by using the finite element method, and clarified what change the stress components underwent according to forms, size, etc., upon evaluating physical values necessary to analyze the sintering behaviors and the thermal stress of non-gradient materials in the zirconia/stainless steel system. Thus, we conducted studies on the optimization of the composition distribution with consideration given to the aforementioned terms 1), 2) and 3). In addition, we will describe the results of producing discoid, sintered functional gradient materials.

2. Evaluation of Sintering Behaviors and Physical Values of Non-Gradient Materials

In the case of producing gradient materials, it is important for the temperature at which sintering shrinkage begins, shrinking speed and the amount of shrinkage to be balanced among non-gradient materials of various compositions during the sintering process. When these conditions vary markedly, the ceramics take distorted forms, and they exfoliate or split between layers that are conspicuously discontinuous. The factors conceivably influencing sintering densification behaviors include powder grain size and its distribution, sintering atmosphere and the speed at which the temperature rises. Figure 1 shows an example of achieving the balance of sintering shrinkage through the coordination of the grain size of material powders and their combination.

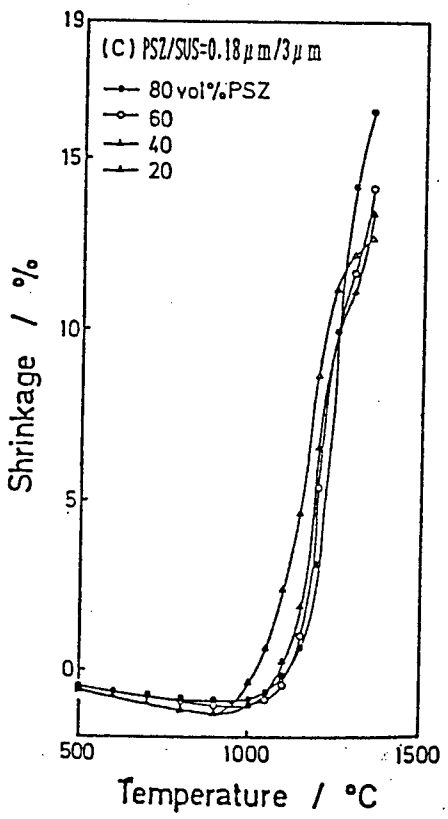

Figure 1. Sintering shrinkage curves of zirconia/stainless steel mixed powder

In every composition, the sintering starting temperature is generally equal, starting at about 900-1,000°C, and the speed and the extent of shrinkage also agree comparatively well. When the shrinkage curves obtained through a combination of various material powders are considered in total, it is thought to be appropriate to use a combination of PSZ powder with an average grain size of 0.18 μm and stainless steel powder with an average

grain size of 3 μm. Even in this case, however, the extent of shrinkage does not always agree completely, and it is necessary to make elaborate plans on the design for composition distribution by such means as changing the composition in a smooth way.

The results of producing non-gradient materials of various compositions by using these powders and measuring their thermal and mechanical properties are given in Table 1.[5,6] A bending strength exceeding 400 MPa was obtained, and it was judged to be comparatively superior from the viewpoint of a microscopic structure as well.

Table 1. Thermal and Mechanical Properties of Zirconia/Stainless Steel Composite Ceramics

	vol%OSZ	20	40	60	80
Relative density	%	96	96.1	97.3	98.1
Bending strength	MPa	608.7	432.9	424.6	541.4
K_a	$MPa \cdot m^{\frac{1}{2}}$	-	9.5	3.9	-
Young's modulus	CPa	189.4	181.1	180.0	183.1
Poisson ratio		0.276	0.278	0.277	0.265
Coefficient of thermal expansion	10^{-6}	16.5	15.3	13.6	10.8
Thermal conductivity	W/m·K	11.7	8.1	4.4	2.4

3. Dependence of Thermal Stress Distribution Upon Forms and Size and Optimization of Composition Distribution

The thermal stress arising in the cooling process from the sintering temperature of 1350°C to room temperature was analyzed by the finite element method (composite structure analyzing program ISAP-6). The analyzing model is an axial symmetric rotator, and the right half of the longitudinal section was divided into elements by use of a square isoparametric element. For various physical values including Young's modulus, Poisson ratio and the coefficient of thermal expansion, we used the values of actual measurements shown in Table 1. We ignored the dependence of the physical values upon temperature, and also plastic deformation. We changed the diameter, the thickness of zirconia and stainless steel layers, the thickness of gradient composition control layers and the form of composition distribution, respectively.

Figure 2 shows the distribution of the axial stress in the cylindrical gradient composition controller, with the zirconia-stainless steel direct junction and the composition changed in stages.

H/d is 1.2. In the case of a direct junction, tensile stress occurs on the ceramic side, markedly exceeding its own tensile strength, with the junction interface in between, and compressive stress arises on the metal side, as already reported. In regard to actual junction samples, too, it is reported that cracks are often observed in the neighborhood where tensile strength is calculated to be greatest. When a gradient composition control layer is introduced, however, stress concentration is eased on the whole, as seen in Figure 2 (b), and the maximum value of the axial stress is reduced effectively

to about half as compared with the case of a direct junction. The maximum stress in a cylindrical form is an axial stress, and the degree of a different stress component arising on the zirconian side is comparatively low.

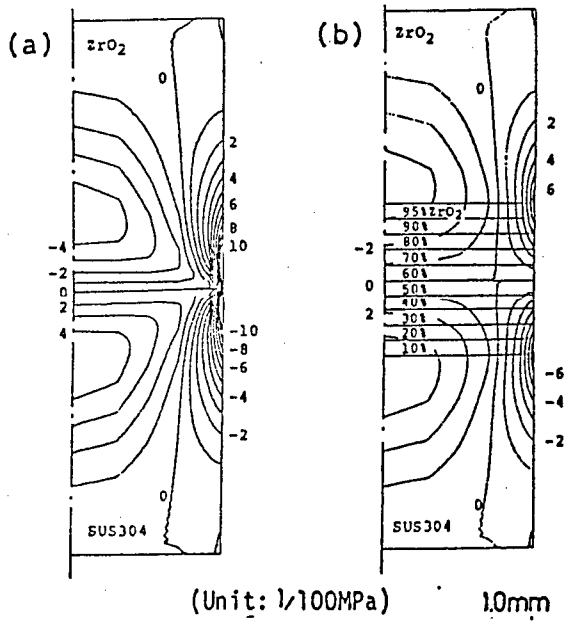

Figure 2. Effects of easing thermal stress in cylindrical gradient composition controller
(a) direct junction, (b) gradient composition control

On the other hand, the distribution of various thermal stress components occurring in cylindrical, functionally gradient materials is shown in Figure 3. H/d is 0.26.

The illustration shows that the axial stress is low inside and that it is concentrated in the peripheral part, the same as the case of the cylindrical gradient composition controller shown in Figure 2 (b). However, the radius and circumferential stress of about the same size as in the case of the axial stress appears, as shown in Figure 3 (b). Both the radius and the circumferential stress are distributed in generally the same way, and they become larger as they come closer to the central axis. Since the point where a material begins to break is presumed to be the part where the maximum tensile stress is placed, it is important to grasp also the state of distribution of other stress components in the case of a discoid material with a higher rate of height than the diameter. Every stress tends to increase as the diameter becomes longer, and this trend is especially conspicuous in the maximum axial, radius and circumferential stresses in zirconic layers.

Figure 4 shows the relationship between the form of composition distribution and a maximum axial stress, with the thickness of a gradient composition control layer as the parameter.

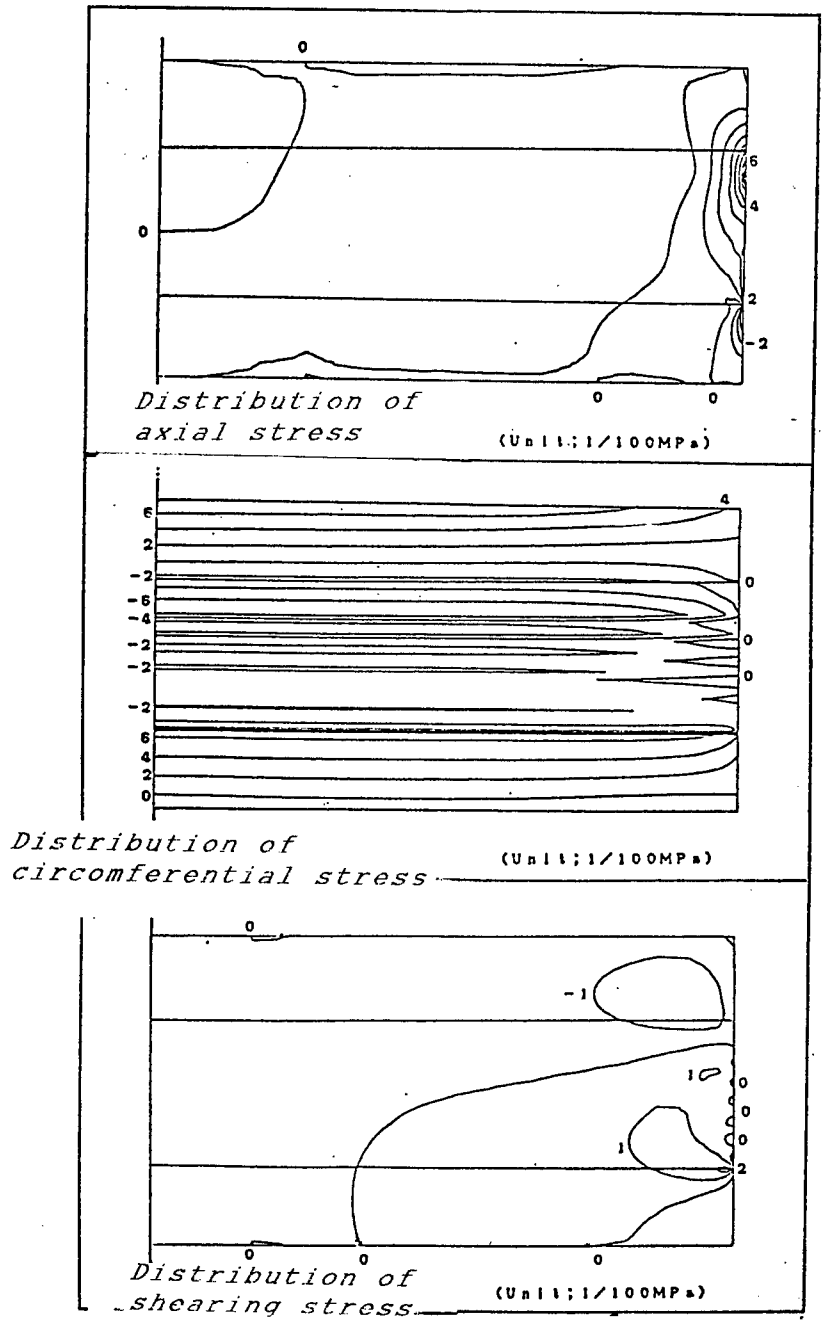

Figure 3. Distribution of thermal stress in cylindrical, gradient composition controller

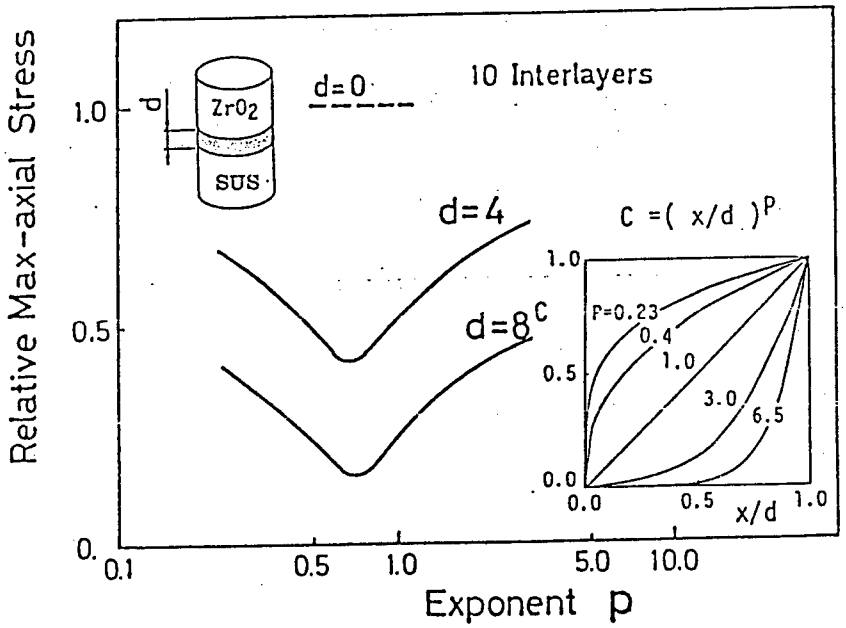

Figure 4. Effects of the thickness of gradient composition control layer and composition distribution upon maximum axial thermal stress

The composition distribution curve is represented by $C = (x/d)^p$ (d: width of composition control layer; x: distance from one end of the composition control layer; p: indice, p = 1 linear, $0<p<1$ convex upward, $1<p$ convex downward). This shows that the greater the thickness of a composition control layer on the whole, the lower the maximum stress, and that the thermal stress is thus reduced effectively. It also suggests that a gradient composition control layer with a certain width is necessary in order to reduce thermal stress. On the other hand, when an indice (p), i.e., the form of composition distribution, is changed with a definite thickness (d) of a composition control layer, p is found to cause the maximum stress to become very small. From Figure 4 it is presumed that the stress becomes the lowest when p is about 0.7, and that the composition distribution in this case is the most appropriate. This result indicates that the composition gradient on the zirconia side, where a tensile stress occurs, had better be made smaller. It can be thought that this will serve as a design curve in the case of controlling gradient composition in order to reduce an axial thermal stress.

Figure 5 shows the relationship between the thickness of zirconia and a stainless steel layer and the maximum stress. This illustration shows that the axial, radius and circumferential stresses tend to decline with the thinning of the zirconia and stainless steel layers. What is to be noted here is that the size relationship between the axial stress and the radius and circumferential stresses is reversed in the vicinity of t = 1.7 mm. When it is more than 1.7 mm, the axial stress becomes greater. Therefore, when a zirconia or a stainless steel layer is more than 1.7 mm thick, a design guideline to minimize the axial stress is considered effective, and

it is thought possible to optimize the composition distribution by the design curve we showed earlier.

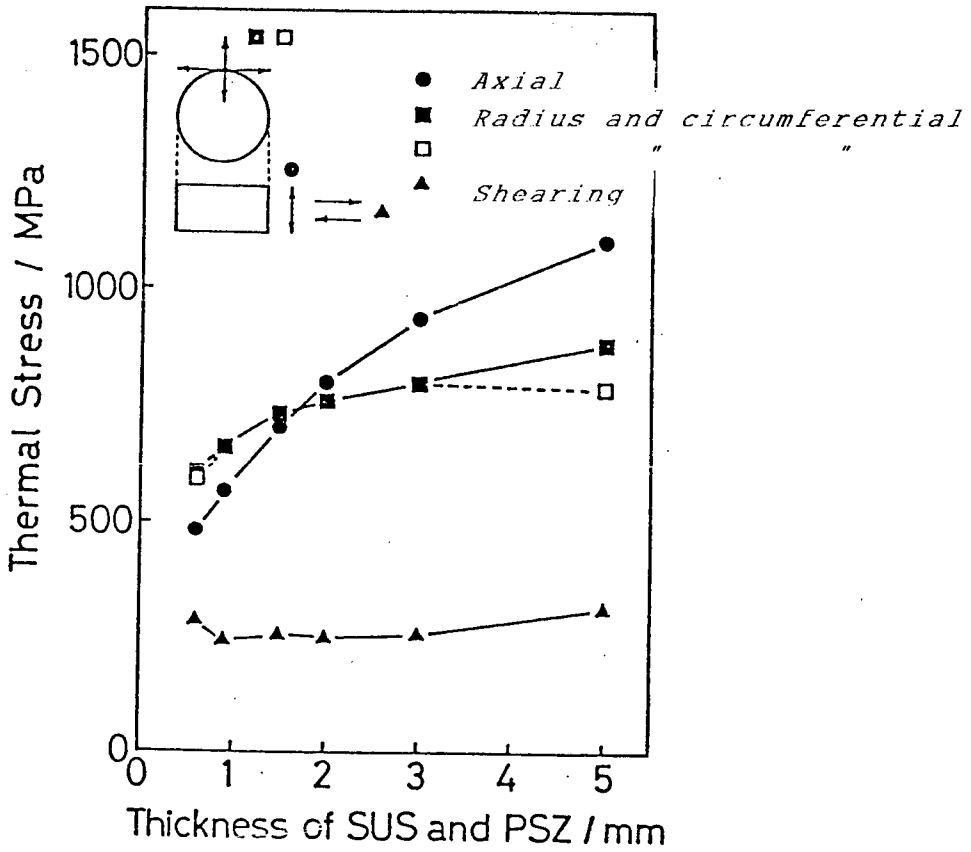

Figure 5. Relationship between the thickness of zirconia and stainless steel layer and maximum stress

4. Production of Discoid, Functionally Gradient Material

On the basis of the results of thermal stress analysis, we produced a discoid, functionally gradient material about 30 mm across and 10 mm high.

The thickness of the zirconia layer and the stainless steel layer was fixed at 2 mm each, and that of the composition control layer at 4 mm. The composition distribution in the composition control layer was established through the use of the design curb given in Figure 4 in an attempt to minimize the axial stress. In addition, some revisions were added in view of the strength, physical values and the balance of sintering shrinkage.[9,10]

For the composition control layer, we used a mixture of PSZ powder with an average grain size of 0.18 μm and stainless steel powder with an average grain size of 3 μm, revealing a comparatively good balance of sintering shrinkage. As the raw material for the zirconia layer, we used 3YPSZ powder with an average grain size of 0.07 μm, taking the strength and thermal shock

into consideration. We also used stainless steel powder with an average grain size of 9 μm in consideration of the sintering shrinkage and forming capacity.

The powders thus determined were subjected to CIP at 200 MPa after they were filled up in step-like composition controllers in the form of a disc, and were metal molded. They were sintered at 1350°C for 1 hour in a vacuum below $1x10^{-4}$ torr.

Figure 6 shows the external appearance of the ceramics and the composition distribution. Reflecting the difference in sintering shrinkage due to composition, they present a somewhat warped shape. On the whole, however, they involve no big defects, showing that they had been sintered with good balance. The microscopic structure of the ceramics revealed a structural change characterized mainly by the dispersion of the constituent layers and the formation of networks.

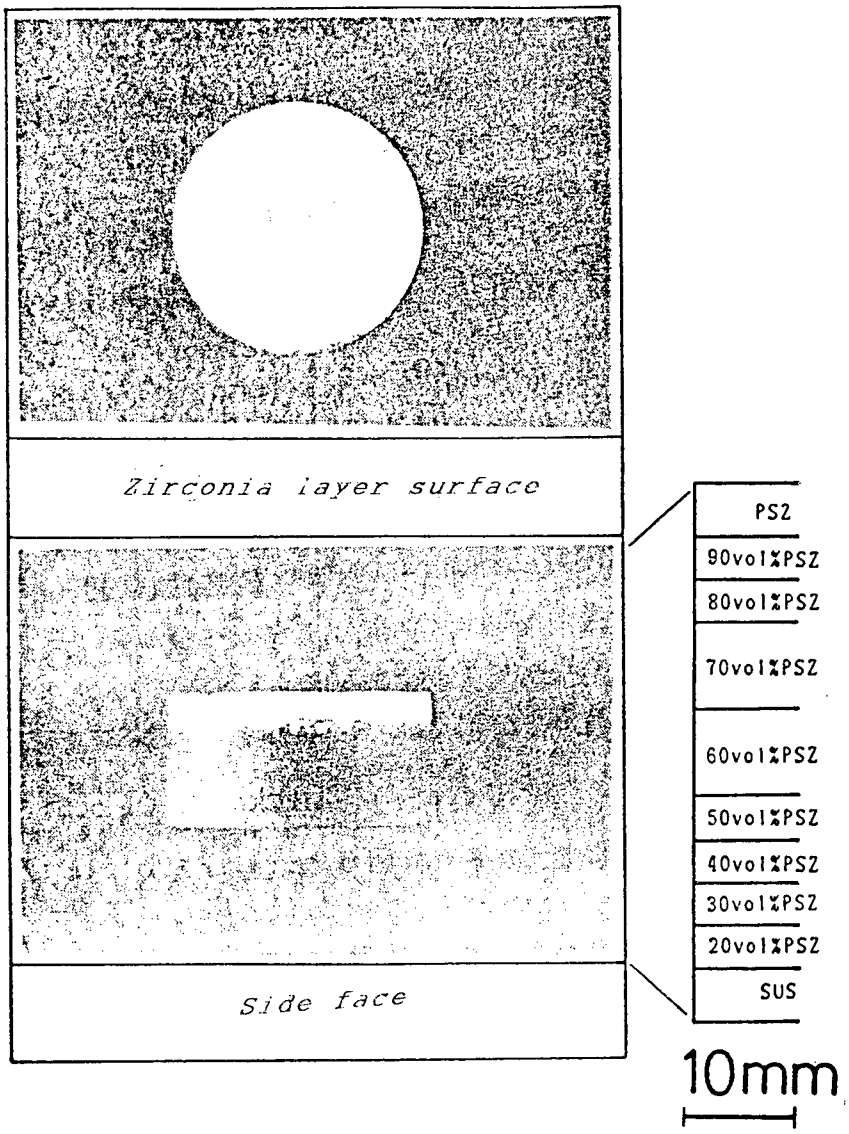

Figure 6. Orbicular, sintered gradient composition control material of zirconia/stainless steel system

In the ceramics not coming under the aforementioned conditions, we observed radial fractures on the zirconia surface due to the circumferential stress, and the occurrence of cracks due to the axial stress.

References

1. Watanabe, Functional Materials, 8, 47 (1988).

2. Watanabe, Kawasaki and Murahashi, Magazine on the Physical Properties of Materials, 1, 36 (1988).

3. Kawasaki and Watanabe, Bulletin of the Japan Institute of Metals, 51, 525 (1987).

4. Iijima, Uchiyama, Kawasaki and Watanabe, Outlines of Speeches by the Japan Institute of Metals, October 1987, p 363.

5. Iijima, Kawasaki and Watanabe, Outlines of Speeches by the Japan Institute of Metals, October 1988, p 363.

6. Saito, Takahashi, Kawasaki and Watanabe, 2nd Symposium on the Nondestructive Evaluation of New Materials and Manufactured Products, 1988, p 187.

7. Okamoto and Suganuma, Sokeizai, 8, 411 (1986).

8. Hamada, et al., Collection of Theses by the Japan Institute of Welding, 4, 73 (1986).

9. Murahashi, Kawasaki and Watanabe, Outlines of Speeches by the Japan Institute of Metals, April 1988, p 130.

10. Iijima, Kawasaki and Watanabe, Outlines of Speeches by the Japan Institute of Metals, April 1989, p 424.

Production of PZT Piezoelectric Functionally Gradient Materials by Temperature Gradient Added Sintering

43067008E Tokyo FGM 89 in Japanese 14 Sep 89 pp 55-59

[Report by Akira Kawasaki and Ryuzo Watanabe of Tohoku University]

[Text] 1. Introduction

In the case of producing sintered, functionally gradient materials, with the sintering temperature for metals differing from that for ceramics, it is necessary to sinter them by adding a temperature gradient that is fully controlled in the region of composition transition. On the other hand, an addition of the temperature gradient is expected to make it possible to obtain ceramics causing the density distribution within a test sample to undergo a continuous change even in the case of a single composition. Therefore, production of functionally gradient materials whose properties will change according to density can be expected.

To date, studies have been carried out mainly on functionally gradient materials of the thermal stress reducing type.[1,2,3] In the research we carried out this time, however, we attempted to reveal the functions of materials through the gradient of density. To start with, we trial-manufactured a sintering furnace enabling materials to be sintered through the addition of a temperature gradient in a region about 5 mm away from the sample surface. In addition, we selected PZT as a material undergoing a change in property according to the density of ceramics.[4,5] We examined the relationship between the density distribution in the ceramics sintered by using this equipment and the temperature gradient added, and also evaluated the piezoelectric properties of the ceramics whose density underwent a continuous change.

2. Trial-Manufacture of Sintering Furnace With Added Temperature Gradient

The trial-manufactured sintering furnace with an added temperature gradient consists of two auxiliary heating furnaces and an infrared-ray heater for the irradiation of the sample surface, as shown in Figure 1. This furnace is based on the idea of controlling a temperature difference and temperature distribution by adjusting the outputs of the auxiliary heating furnace and the infrared-ray heater, upon heating the entire sample to the sintering starting temperature.

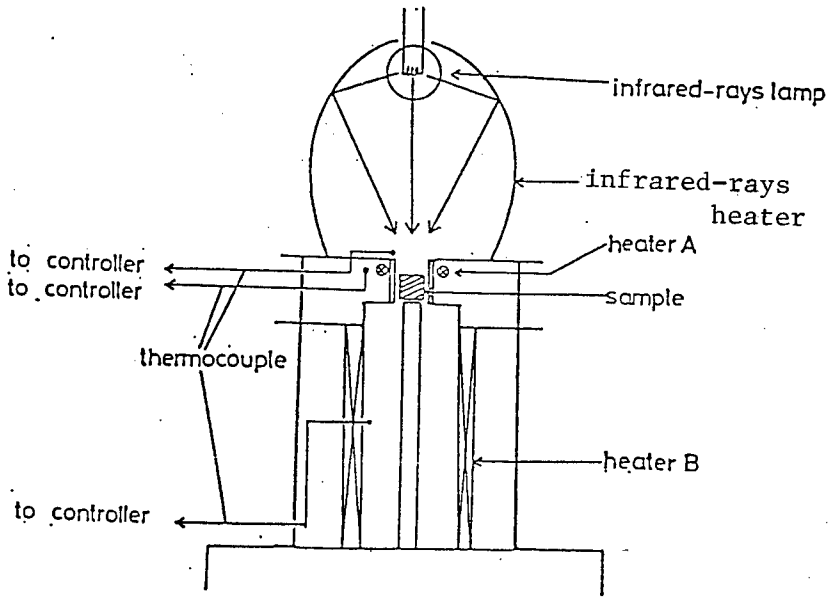

Figure 1. Sintering furnace with added temperature gradient

However, in the case of actually sintering a compressed powder mold, it is very difficult to directly monitor the temperature distribution in the test sample. Therefore, it is necessary to adopt the method of previously quantifying the temperature distribution in the specimen, with the temperatures set in three furnaces as parameters, and establishing the outputs of the furnaces on this basis according to the sintering conditions. The factors influencing the temperature distribution in the specimen include not only the installation of the three heating furnaces but also the position of the specimen. In this research, however, we considered the position of the specimen as an established fact. The positional relationship between the heater and the specimen and the position wherein a thermocouple is inserted for temperature measurements are shown in Figure 2.

Figure 3 shows a change in the temperature distribution in the specimen when the temperature in the heating furnace (A) is fixed at 300°C and the fixed temperature in the heating furnace (B) is changed.

When the specimen is heated with only the heating furnace (A), the inside of the specimen is heated almost uniformly. When it is heated with the furnace (B), on the other hand, the specimen is heated from the lower part, and therefore the temperature becomes gradually higher in the lower part than in the upper part. What is characteristic is that the temperature distribution in the specimen is linear, and that there is a linear relationship between the set temperature of the heating furnace and the specimen temperature under any heating conditions. Therefore, the temperature distribution in the specimen can be presumed when the specimen temperature and the temperature distribution in the specimen are indicated by a linear expression for the set temperature and the distance from the specimen surface.

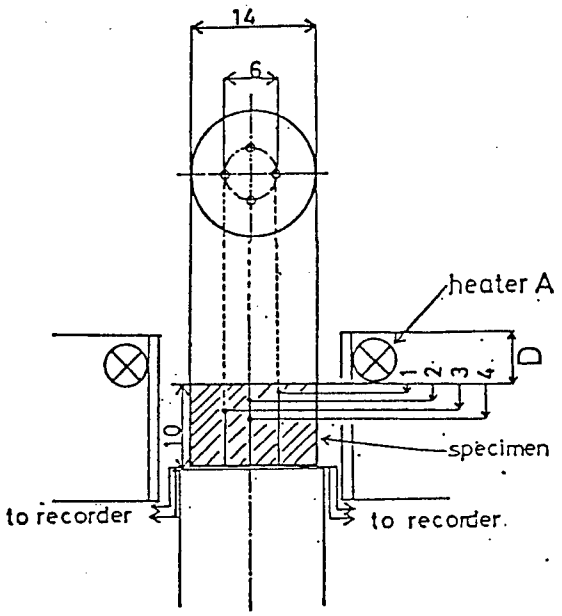

Figure 2. Positions for the installation of compressed powder mold and for the insertion of thermocouple (D = 6 mm)

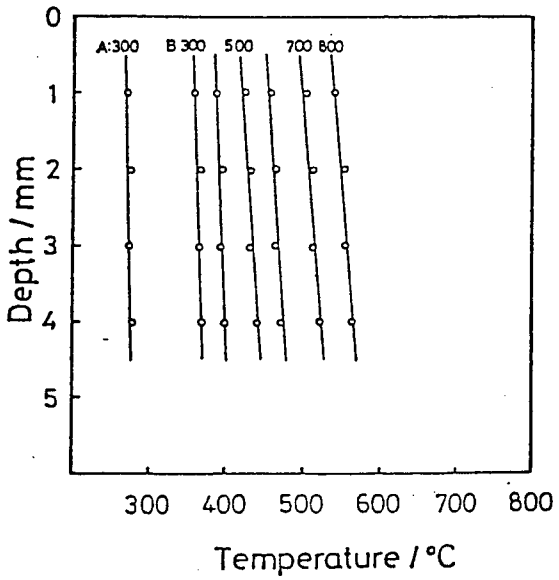

Figure 3. Temperature distribution in a specimen when heated with heating furnaces (A) and (B)
(The vertical axis represents the distance from the specimen surface. A:300 is a set temperature in the heating furnace (A) and the others result from adding the heating furnace (B))

Figure 4 shows an example of temperature distribution in the case of comprehensive heating with three furnaces.

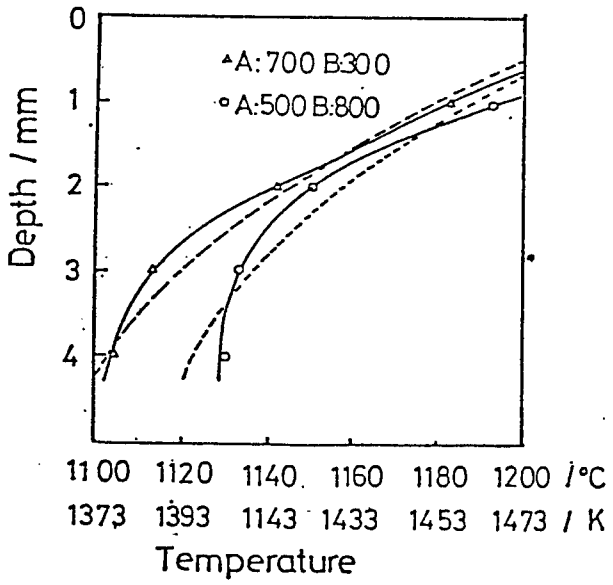

Figure 4. Temperature distribution in a specimen during comprehensive heating
(The vertical axis represents the distance from the specimen surface, and the numerical figures (A) and (B) represent the set temperatures of heating furnaces (A) and (B))

The heating furnaces (A) and (B) are installed so that the sample temperature at the depth of 1 mm before infrared heating will become about 750°C. The amount of the added infrared heating is the same. The infrared heating causes the surface temperature of the specimen to rise rapidly and brings about a temperature gradient toward the inside of the specimen. The higher the temperature gradient in the specimen before the addition of the infrared heating, the higher the temperature gradient when the infrared heating is added. It was also found that a difference in the added temperature gradient became greater with an increase in the depth from the upper surface of the specimen. When infrared heating is added, the temperature distribution in the specimen becomes nonlinear. When a distribution function is applied, however, it can be expressed through its addition to the linear expression shown in Figure 3, although a correction term is necessary. Thus, it was found possible to estimate the temperature status in the specimen from the conditions for installing the heating furnaces.

The temperature of the sample surface in Figure 4 is 1476°C, and there is a difference of 80°C between the depths of 1 mm and 4 mm. It is conceivable that there is a difference of more than 200°C from the sample surface.

3. Sintering of PZT Ceramics With the Addition of Temperature Gradient

3.1. Methods of Experiments

The powder provided for the test was PZT, a product of Kyoritsu Ceramics, Ltd. It was preliminarily molded under the pressure of 150 MPa through the use of a 14 mm metallic mold, and then it was subjected to CIP with the pressure of 200 MPa.

The sintering process with the addition of a temperature gradient was effected under the two conditions given in Figure 2, with which the temperature distribution was actually measured. The temperature at the depth of 1 mm of the specimen was provided in the neighborhood of 1180°C, slightly higher than the sintering temperature. The ceramics produced with a larger amount of added temperature gradient are hereinafter called (a), and those produced with a smaller amount of added temperature gradient are to be called (b).

The macroscopic shrinkage modulus in the diametrical direction was measured through a photograph taken from the side face of the ceramics. After grinding the cross section of the ceramics with waterproof polishing paper, we observed their structure with an optical microscope, and at the same time measured the distribution of the relative density with an image analyzer. With regard to piezoelectric properties, we carried out polarization treatment at 10 KV and at the temperature of 200°C for 1 hour, and thereafter measured resonant frequency (fr) and antiresonant frequency (fa) by using constant current circuits.

3.2. Results and Observations

Figure 5 shows a photo of the external appearance of ceramics sintered with a temperature gradient added. The illustration shows that the amount of shrinkage changes continuously from the upper part of the specimen to its lower part. Also, the amount of shrinkage near the base is smaller in (a) than in (b), clearly revealing the difference in the added temperature gradient.

The result of measuring the average shrinkage modulus in the radius direction from the sample surface at intervals of 1 mm is given in Figure 6. Evidently, the specimen with a larger amount of the added temperature gradient shows a greater change in shrinkage modulus, corresponding to the result of the temperature distribution in Figure 4.

Figure 7 shows the relative distribution of density sought by an image analysis. The density distribution in the part 3 mm away from the central axis, where the temperature distribution was measured, reveals a marked difference from the depth of more than 2 mm or so, and this well agrees with the result of measurement. On the central axis, on the other hand, there is no great difference between (a) and (b) in the distribution of density. It is therefore conceivable that the temperature gradient is not uniform from the sample surface to the inside. In addition, the density tends to become higher in the central part of the sample surface, and it is presumed that the temperature near the center is rather high.

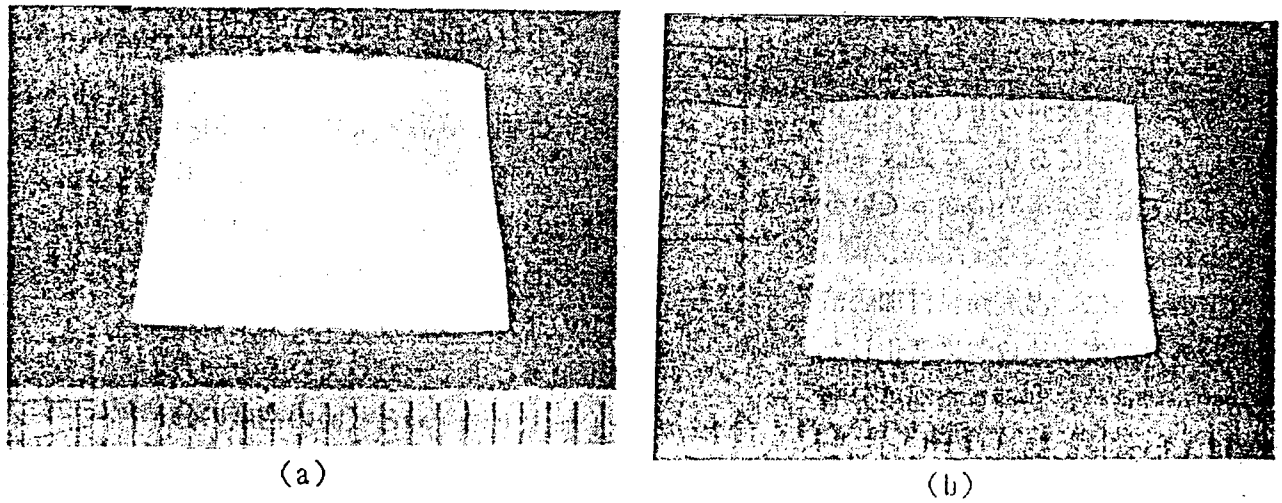

Figure 5. External appearance of PZT sintered with temperature gradient added
(a) A: 700°C, B: 300°C
(b) A: 500°C, B: 800°C

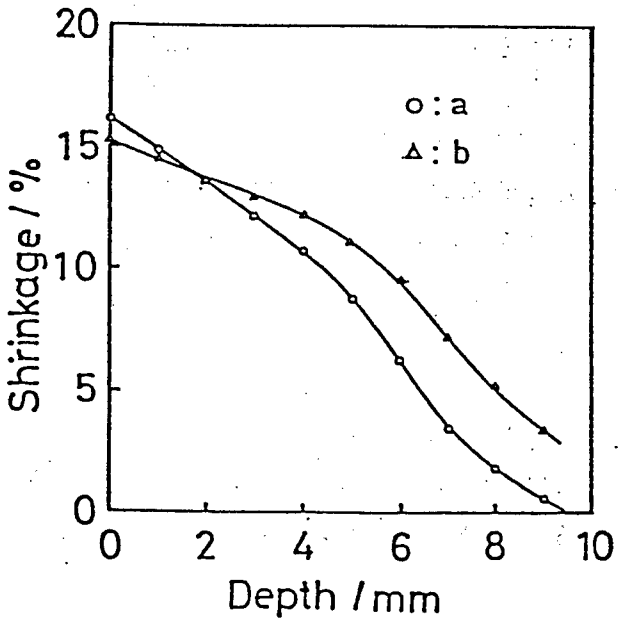

Figure 6. Change in macroscopic shrinkage modulus in ceramics with temperature gradient added
(The horizontal axis represents the distance from the sample surface)

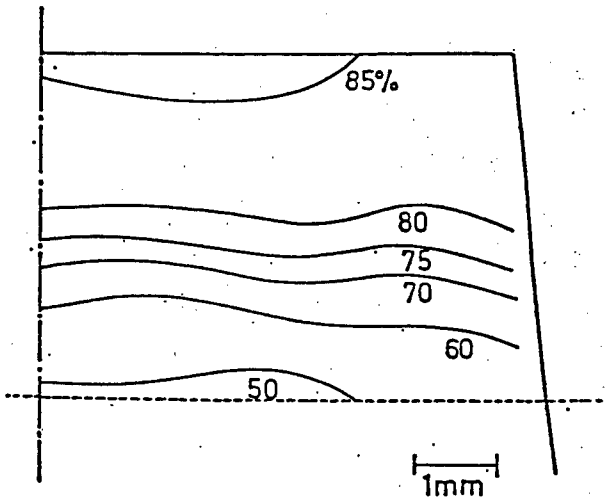

Figure 7. Distribution of relative density in PZT cross section sintered with temperature gradient added

As mentioned above, ceramics undergoing a continuous change in density is obtained when temperature gradient added sintering is carried out, and the density becomes gradient in line with the controlled temperature distribution. However, the change in the density distribution from the sample surface toward the depth is not uniform. The density is high in the central part of the surface, and the density change along the central axis tends to become greater than in the side face. This is thought to be due to the properties of trial-manufactured sintering furnace equipped with a temperature gradient.

Figure 8 shows an example of frequency characteristics measured by using constant current circuits. The frequency shown by the lower tip of the peak near 200 Hz is fr, and the one shown by the upper tip of the peak is fa. The peak showing fa is observed in every specimen, and it reveals piezoelectric properties. On the other hand, small peaks not found in general piezoelectric materials are observed at the right and the left of the peaks showing fa and fr. This indicates that a peculiar resonance in terms of a refraction mode occurs as against the radial mode that is a general resonance in the diametrical direction. The refraction mode occurs when the expansion and contraction in the upper part of a piezoelectric material are different from those in the lower part. Generally, it is generated by a bimorph structure that causes two piezoelectric materials differing in the direction of expansion and contraction to stick together. Because of the sintering process accompanied by a temperature gradient, however, the amount of expansion and contraction is larger in the upper part because of high density, while it is small in the lower part because of low density. It is therefore conceivable that resonance with a refraction mode took place in a single piezoelectric material.

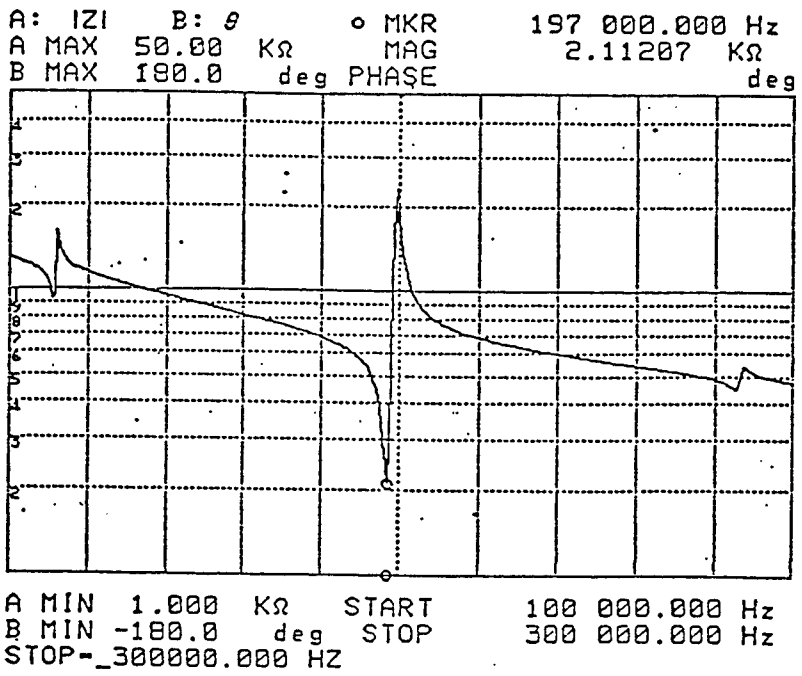

Figure 8. Piezoelectric properties of PZT that is sintered with temperature gradient added

References

1. Report of Investigations on Basic Technologies To Reveal Functions Through Complexes and To Ease Thermal Stress, Science and Technology Information Foundation, 1987.

2. Kawasaki and Watanabe, Bulletin of the Japan Institute of Metals, 51, 525 (1987).

3. Watanabe, Kawasaki and Murahashi, SOZAI BUSSEIGAKU ZASSHI, 1, 36 (1988).

4. P. G. Lucuta, F. Constantinescu and D. Barb, J. Am. Ceram. Soc., 68, 533 (1985).

5. M. Kahn, J. Am. Ceram. Soc., 68, 623 (1985).

Synthesis of SiC-C Functionally Gradient Materials by the CVD Method

43067008F Tokyo FGM 89 in Japanese 14 Sep 89 pp 61-68

[Report by Makoto Sasaki, Akira Ohkubo and Toshio Hirai of the Metallic Materials Research Laboratory of Tohoku University; Wang Yucong of Tohoku University Graduate School; Toshiyuki Hashida and Hideaki Takahashi of Tohoku University Engineering Department; and Tohru Hirano of Daikin Kogyo Co., Ltd.]

[Text] 1. Introduction

Many studies have been conducted on plate-shaped in-situ composites synthesized by the CVD (chemical vapor deposition) method, with the distribution phase distributed uniformly. These CVD in-situ composites have uniform properties covering all the materials. Against these, composites having component gradients from one side of a plate-shaped material to the other, that is, having gradient functions [functionally gradient materials (FGM)] involve multiple functions and superior properties in one material.

Recently, materials that can be used in an environment causing one side of a substance to be exposed to an oxidized atmosphere with a high temperature exceeding 1600K, while the other side is cooled to 300K, bringing about a temperature difference of more than 1000K in the substance, are needed as materials for aircraft. Conventional materials with uniform composition cannot withstand such a severe environment. Therefore, we researchers attempted to synthesize SiC/C·FGM by the CVD method, with its functions made gradient by continuously controlling the composition from SiC to C, as a material provided with oxidation resistance and high-temperature strength on one side and easy processibility and high thermal conductivity on the other, and involving low Young's modulus.[1]

2. Design for SiC/C·FGM

On the supposition of producing a combustion nozzle, we investigated a state of plane stress when there is a temperature of 1300K inside an infinite cylinder measuring 10 mm in thickness and 95 mm in inner radius and 300K outside the cylinder, and when a temperature difference of 1300K arises in this case.[2]

When this infinite cylinder consists of a SiC single phase, the thermal stress arising on the inner plane of the cylinder becomes about three times as strong as the breaking strength of SiC--650 MPa. In this case, it is assumed that the combustion nozzle consisting of a SiC single phase may be broken by the thermal stress.

Therefore, for the purpose of lowering the thermal stress as much as possible, we sought to ascertain, through calculations, what change would take place in the temperature distribution toward the depth, stress distribution, Young's modulus and the ratio of stress (ratio between strength and inner stress) when the component ratio [SiC/(SiC+C)] toward the depth of this infinite cylinder is changed.

C is strongly anisotropic, showing a low thermal conductivity in the interlayer (c-axis) direction and a high rate of thermal expansion. In the case of CVD-C, the c axis is oriented in parallel with the direction of growth, and therefore the thermal stress toward the depth of the infinite cylinder is to be calculated. As to the physical value of CVD-C, therefore, we used the value in the c-axis direction. In making calculations, we used Kerner's rule of mixture for thermal conductivity, Young's modulus and the rate of thermal expansion. As for the rule of mixture in regard to strength, we used the harmonic mean rule, and established binding conditions in such a way that both the inside and the outside are to be bound by stress.

As a hypothesis for calculations, we presumed that the portion from the inside surface to the depth of 1 mm formed a single SiC phase, and that the part from the depth of 1 mm to 10 mm consisted of SiC/C·FGM. Thus we calculated the stress occurring in the SiC/C·FGM that involves all sorts of composition distribution according to temperature gradient conditions. As for the results of calculations concerning various setting conditions, Figure 2.1 shows the stress distribution, temperature distribution and Young's modulus when the rate between the strength and the internal stress is less than 1, that is, when the stress arising in SiC/C·FGM is not above the strength of a single SiC phase and therefore it is not expected to break. The composition distribution in that case is shown in Figure 2.2.

3. Methods of Experiments

3.1. Method To Synthesize SiC/C·FGM

The relationship between the flow ratio of material gas and the isolate carbon in the generated SiC-C composite material is shown in Figure 3.1.1. In addition, the relationship between the composition of the composite material and its density are given in Figure 3.1.2.[3]

We conducted CVD experiments on the basis of these basic data. SiC/C·FGM with composition distribution close to that shown in Figure 2.2 was synthesized in the way described below. The CVD equipment used for the experiments is shown in Figure 3.1.3. As a raw material, we used the $SiCl_4$-CH_4-H_2 system, with the temperature of the $SiCl_4$ vessel kept at 20°C and with H_2 as a carrier. We held the substrate graphite in a graphite

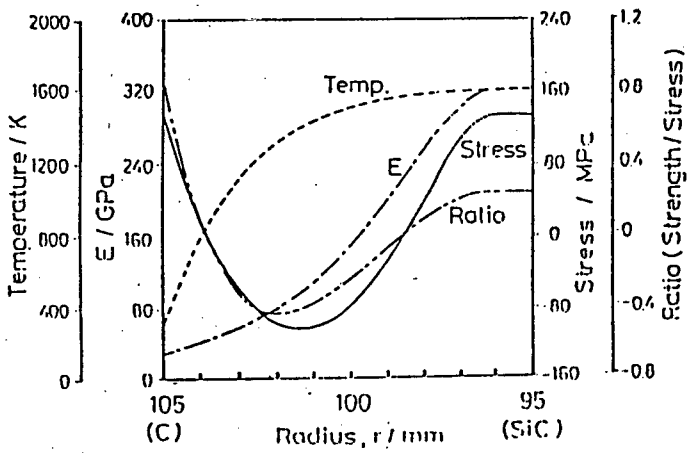

Figure 2.1. Results of calculations of stress distribution, temperature distribution, etc.

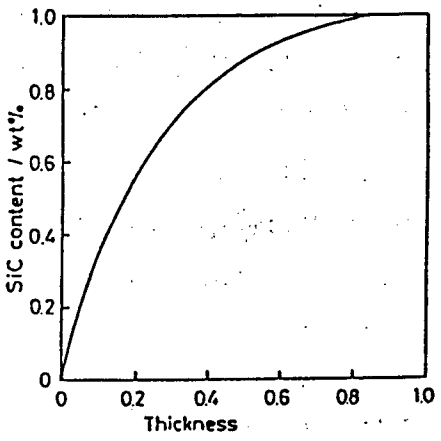

Figure 2.2. Results of calculations of optimum composition distribution

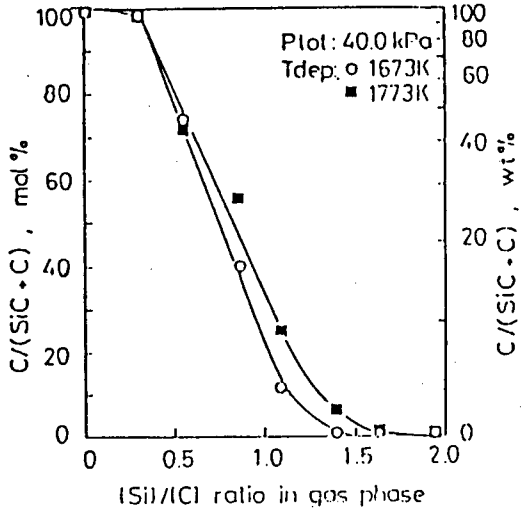

Figure 3.1.1. Dependence of isolate gas upon gas composition

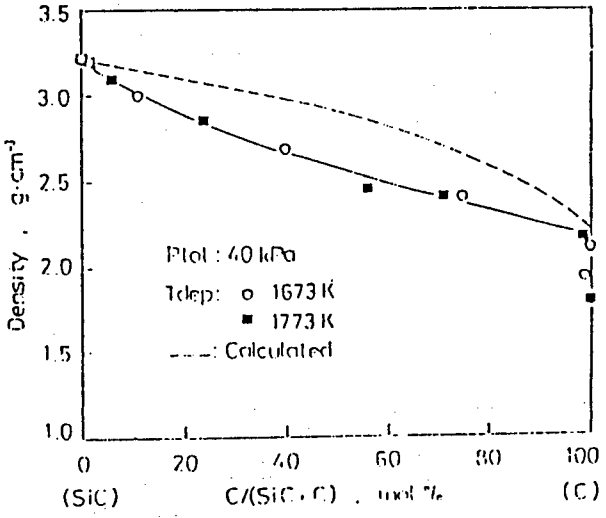

Figure 3.1.2. Relationship between the composition of precipitation and its density

heater heated through high frequency induction, and introduced material gas from the lower part. We continuously changed the flow of the material gas by using a sequencer. As for all the pressure in the furnace, we kept it constant using pressure control equipment. The CVD conditions are given in Table 3.1.1. The synthesizing temperatures were 1673K and 1773K, and the entire gas pressure was fixed at 1.3 kPa. Figure 3.1.4 shows the time change in the rate between Si and C in the material gas used for the experiments, with the synthesizing time as 9 ks.

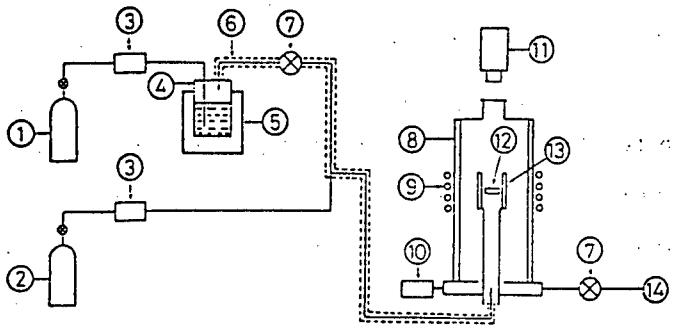

Figure 3.1.3. CVD equipment
(1) Carrier gas; (2) reaction gas; (3) mass flowmeter; (4) liquid raw material vessel; (5) thermostatic bath; (6) ribbon heater; (7) pressure regulator; (8) reactor of the water cooling type; (9) work coil; (10) pressure gauge; (11) optical pyrometer; (12) substrate; (13) heater; (14) exhaust pump

Table 3.1.1. CVD Conditions

Synthesis temperature	Tdep	K:	1673 1773
Inter-furnace pressure	Ptot	kPa:	1.3
Gas flow	10^{-6}	m sec^{-1}:	
		$SiCl_4$:	0 → 1.7
		CH_4 :	6.7 → 1.3
		H_2 :	0 → 5.0
Synthesizing time	1 dep	ks:	9

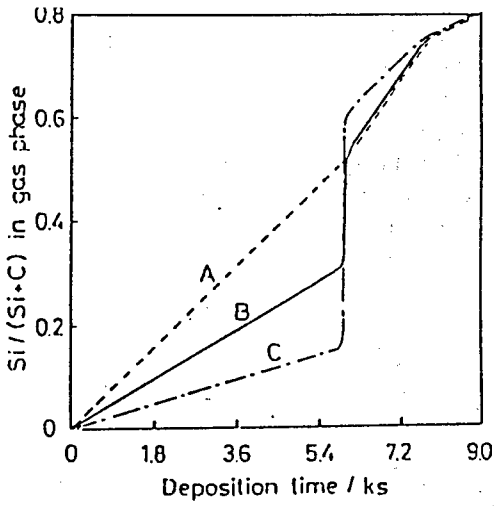

Figure 3.1.4. Change in material gas composition during synthesis

3.2. Measurement of Conductivity

We measured the conductivity of SiC and SiC/C·FGM in an Ar atmosphere within the limit of 1200K from the room temperature, using the DC four-terminal method.

3.3. Evaluation of Thermal Impact Resistance

We conducted thermal impact resistance tests by means of 50W CO_2 laser. In the experiments, we carried out repeated heating 65 times, each time continuing irradiation for 6 seconds and suspending it for 6 seconds. Thus, we examined the dependence of AE signals upon critical output density. In addition, we observed cracks on the sample surface after the tests. We also kept the temperature of test pieces at 1243K and observed how the film exfoliated after being thrown into 273K water.

4. Results of Experiments

4.1. Synthesis of SiC+C·NFGM

Figure 4.1.1 shows the dependence of the C content in SiC+C·NFGM, synthesized at 1773K and at 1.3 kPa by the use of an $SiCl_4$-CH_4-H_2 system, upon the composition of the material gas. When compared with $SiCl_4$-C_3H_8-H_2 system (1773K and 40 kPa), the gradient of the curve is higher in the case of the CH_4 system.

In order to control the C content in FGM, therefore, it is necessary to control the Si/C ratio in the material gas more accurately. Figure 4.1.2 shows the relationship between the speed of growth and the C content in the deposition, revealing the same trend as in the case of the C_3H_8 system. As shown in Figure 4.1.3, the result of thermodynamic equilibrium calculations

revealed that changes of Tdep and Ptot cause a change in the conditions under which C begins to coprecipitate in SiC, even when the Si/C ratio is made constant in the material gas.

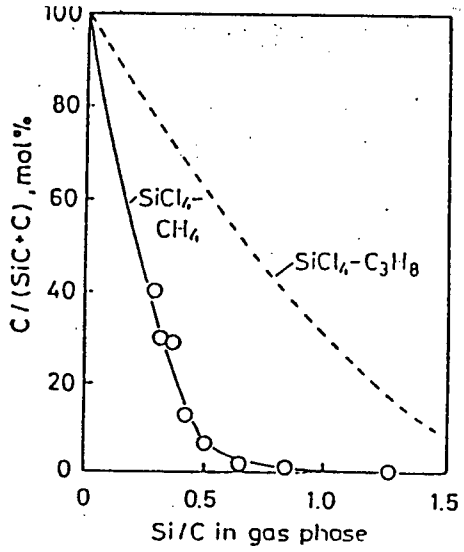

Figure 4.1.1. Relationship between the C content in SiC+C·NFGM and the density of material gas
$SiCl_4$-CH_4 : 1773K, 1.3 kPa
$SiCl_4$-C_3H_8: 1773K, 1.3 kPa

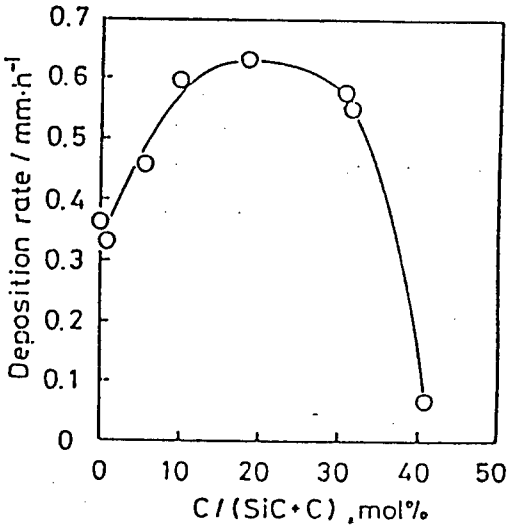

Figure 4.1.2. Growth speed of thickness of SiC+C·NFGM
$SiCl_4$-CH_4: 1773K, 1.3 kPa

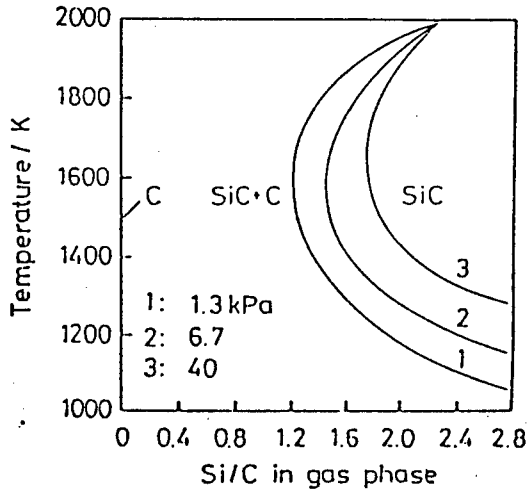

Figure 4.1.3. CVD phase

It can be said that a higher Ptot is suited to synthesize SiC/C·FGM, because the lower the Ptot, the wider the area for SiC alone to grow.

4.2. Relationship Between C Content of SiC+C·NFGM and Its Conductivity

We synthesized CVD-SiC·NFGM under the conditions of Tdep = 1573-1773 and Ptot = 0.13-6.7 kPa, with the fixed values of $FR(SiCl_4)$ = 100 cc/min, $FR(H_2)$ = 300 cc/min and $FR(CH_4)$ = 80 cc/min. As a result of using X-ray diffraction, we detected no isolate C. Moreover, the density was generally close to the theoretical density of SiC.

The result of measuring the conductivity of these samples at 333K is given in Figure 4.2.1.

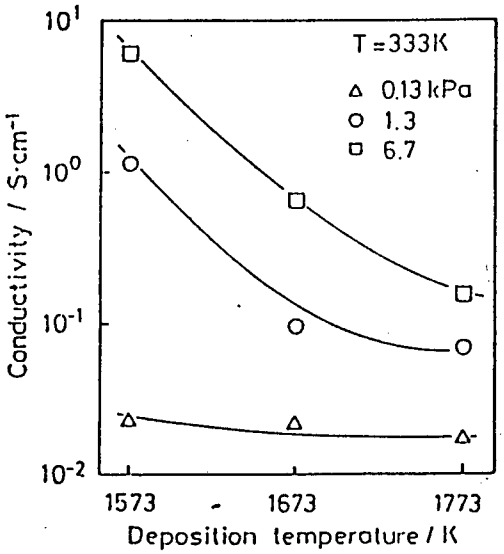

Figure 4.2.1. Conductivity of SiC·NFGM at 333K

We also examined the relationship between the C content in SiC+C·NFGM that was synthesized through changing the value to $FR(CH_4)$ = 80-280 cc/min at 1773K and 1.3 kPa, and its conductivity. From Figure 12 [as published] it is conceivable that the lower the Tdep and the higher the Ptot, the easier it is for C to coprecipitate in SiC. This agreed well with the result of the thermodynamic equilibrium calculation, given in Figure 4.1.3.

4.3. Synthesis of SiC/C·FGM

The composition distribution in the cross section of SiC/C·FGM is shown in Figure 4.3.1. In pattern C with a small amount of Si supply, SiC became rich and gradient composition was not realized. In the case of the sample synthesized at 1773K and 1.3 kPa (pattern A), the entire film was porous. Pores were observed near the substrate of a sample synthesized at 1673K and 1.3 kPa (pattern B).

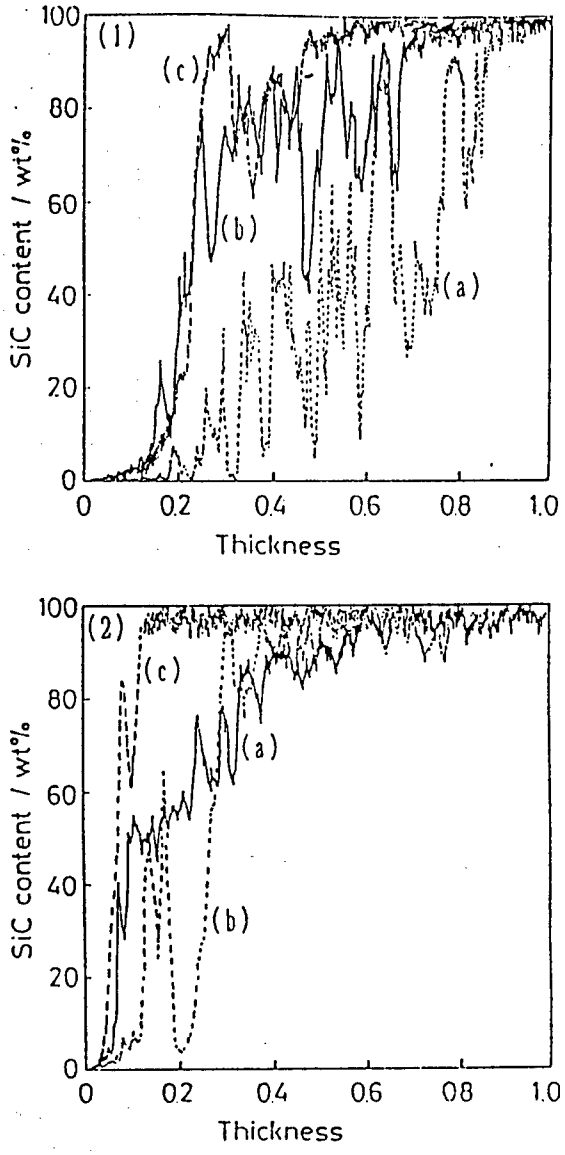

Figure 4.3.1. Composition distribution in the cross section of SiC/C·FGM
(1): 1773K-1.3 kPa, (2): 1673K-1.3 kPa,
(a): pattern A, (b): pattern B,
(c): pattern C

The samples synthesized at 1773K and 1.3 kPa (pattern B) and at 1673K and 1.3 kPa (pattern A) were the closest to the composition distribution exhibited when stress was the smallest. As an example, the structural photo of a sample synthesized at 1773K and 1.3 kPa (pattern B) is given in Figure 4.3.2 [not reproduced]. The precipitation surface constituted a pebble-like structure peculiar to SiC that is synthesized under this condition. As a result of SEM observation of the cross section, it was found to be a comparatively dense film on the whole, though the vicinity of the center

of the film was somewhat porous. These pores are presumed to rather contribute to easing the stress.

Figure 4.3.2 (C) shows an EPMA X-ray image of Si, revealing that Si underwent a continuous change. We were thus able to synthesize materials which are componently gradient from C to SiC, by continuously controlling the Si/C ratio in raw materials by the CVD method, for which $SiCl_4$-CH_4-H_2 was used as a raw material.

4.4. Conductivity of SiC/C·FGM Surface

We attempted to synthesize SiC/C·FGM under the conditions of Tdep = 1673-1773K and Ptot = 1.3-6.7 kPa, with the synthesizing time (t_d) fixed at 9 ks. Figure 4.4.1 shows the elapse change in the Si/C ratio in the material gas used for the experiments.

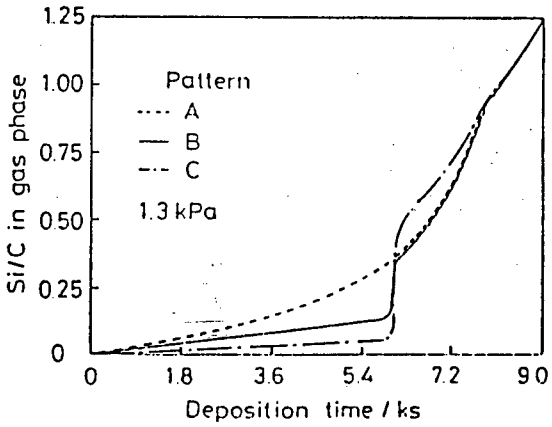

Figure 4.4.1. Elapse change in the density of material gas during FGM synthesis (Ptot = 1.3 kPa)

The calculation of the Si/C ratio in the vicinity of the substrate is given in Figure 4.4.2, on the supposition that the diffusion in a CVD furnace is uniform. It is conceivable that when Ptot becomes high, a time lag occurs between the Si/C ratio near the substrate and the Si/C ratio on the supply side. From Figure 4.4.2, it is assumed that the higher the Ptot becomes, the Si/C ratio near the substrate will become lower, making it easy for C to coprecipitate to SiC. From the comparison between the conductivity in the FGM precipitation surface and the conductivity of the SiC·NFGM (Figure 4.2.1) synthesized with a fixed composition of material gas, it can be said that the conductivity in the surface of FGM synthesized with a high Ptot becomes high and that the FGM surface tends to form SiC+C. In the case of synthesizing SiC/C·FGM, it is necessary to consider such effects of gas diffusion as well.

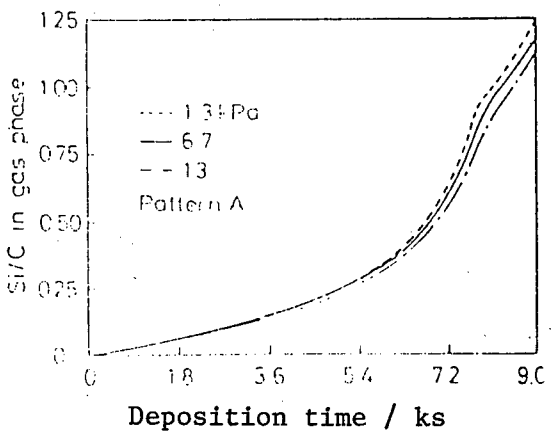

Figure 4.4.2. Dependence of material gas density upon Ptot during FGM synthesis (pattern A)

4.5. SiC/C·FGM Resistance to Thermal Shock

We tested SiC·NFGM, SiC+C·NFGM and SiC/C·FGM for resistance to thermal shock with a laser heating thermal shock tester. As a result, neither NFGM nor FGM were cracked even when repeatedly heated by laser, as shown in Table 4.5.1, and there was no significant difference between the two. The AE signals on this occasion are shown in Figure 4.5.1, and a SEM photo of the sample surfaces after the heating of laser is given in Figure 4.5.2. The AE signals on that occasion were not detected except on a noise level, and it was found that they did not break even when subjected to forced heating.

As a result of a forced cooling test conducted by throwing them into water after holding them at 1243K for 5 minutes, only the FGM did not exfoliate.

Table 4.5.1. Resistance of SiC/C Composite Materials to Thermal Shock

Materials		Forced heating[1]	Forced cooling[2]
		Occurrence of cracks	Film exfoliation
NFGM	SiC	Occurred	Occurred
	SiC+30mol%C	Did not occur	Occurred
	SiC / SiC+30mol%C	Occurred	Occurred
FGM	SiC/C	Did not occur	Did not occur

1) Laser heating thermal shock testing method
   6 sec on - 6 sec off (789 sec)
2) Aquatic rapid cooling method
   1243K —(5 min)— 273K

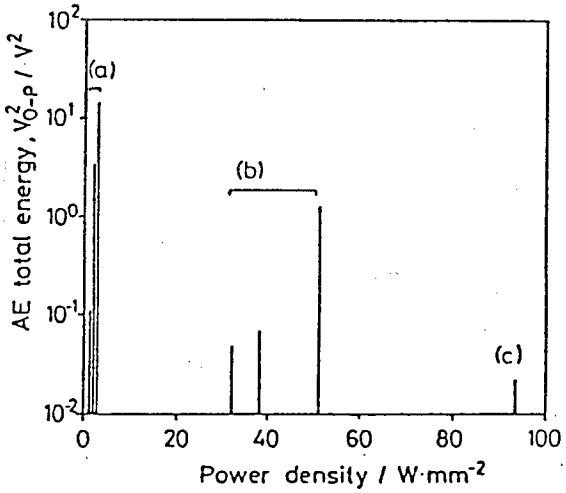

Figure 4.5.1. Dependence of AE signals upon critical output density during laser thermal shock test
(a) ZrO_2-3mol%Y_2O_3 (2 mm^t)
(b) ZrO_2(0.1 mm^t)/NiCrAlY(0.1 mm^t)/Cu(5 mm^t)
(c) CVD-SiC·NFGM(0.4 mm^t)/C(5 mm^t)

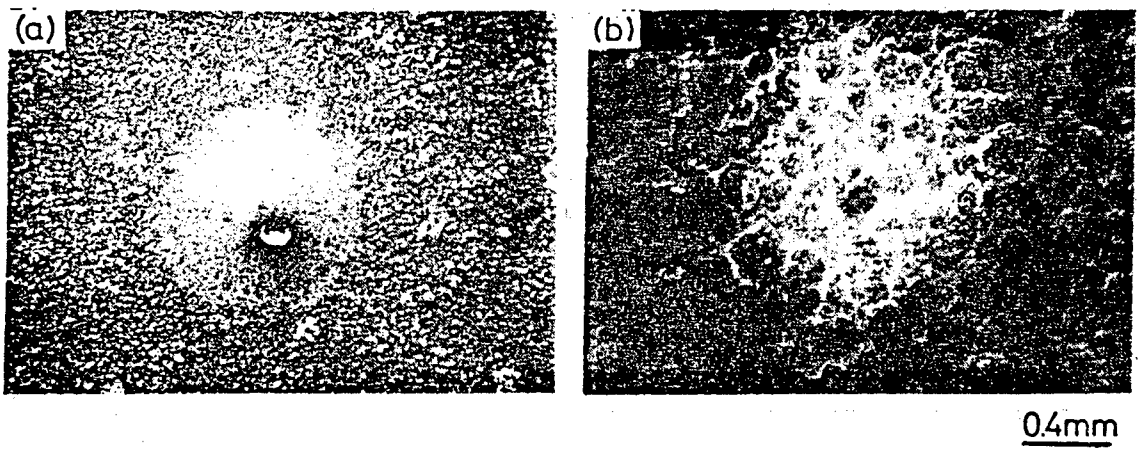

Figure 4.5.2. SEM photo of sample surfaces after laser thermal shock test (1773K, 1.3 kPa)
(a) SiC·NFGM, (b) SiC/C·FGM (pattern B)

References

1. Makoto Sasaki and Toshio Hirai, Outlines of Speeches at 103rd Autumn Seminar of the Japan Institute of Metals, (1988), p 433.

2. Makoto Sasaki, Wang Yucong, Tohru Hirano and Toshio Hirai, Scientific Journals Published by the Japan Institute of Ceramics, 97 (1989), 539-43.

3. Wang Yucong, Makoto Sasaki and Yoshio Hirai, Outlines of Speeches at the 102nd Spring Symposium of the Japan Institute of Metals, (1988), p 261.

4. Wang Yucong, Makoto Sasaki, Takashi Goto and Hoshio Hirai, J. Mat. Sci., contributions under way.

Production of SiC/C Functionally Gradient Materials--Study of Size Increase by the CVD Method

43067008G Tokyo FGM 89 in Japanese 14 Sep 89 pp 69-73

[Report by Seiichi Uemura, Yoshio Sohda and Yukinori Kude of Nippon Oil]

[Text] 1. Introduction

We see examples of FGM's in nature, but our major objective regarding FGM's lies in artificially synthesizing them on the basis of techniques for materials designing and applying them to fields including space shuttles, which we have so far been unable to reach with conventional materials. Therefore, an FGM project is characterized by making designs for materials by using data on basic physical properties through NFGM's and synthesizing materials on the basis of the results thereof. Because of such backgrounds, it is necessary for the groups in charge of synthesis to pursue both the development of synthesizing methods and the production of test pieces for materials designing simultaneously, side by side. With regard to the CVD method, joint research has been carried out up to the present, with the Hirai Laboratory taking charge of the former and Nippon Oil taking care of the latter. The objective of this research is to study conditions for the increase of size based on the results of the investigations by the Hirai Laboratory and produce test pieces for the adoption of design data. This is also one step toward 300 mm x 300 mm FGM's for the second term.

2. Methods of Experiments

2.1. Synthesis

We adopted the hot-wall form for the equipment, taking the scaling up and coating for C/C composites, etc., into consideration. The conditions for synthesis are shown in Table 2.1.1, and the equipment is outlined in Figure 2.1.1.

2.2. Evaluation

(1) Mechanical properties.: NFGM's were supplied to the properties evaluation group as samples for MSP tests, bending tests, and breaking tenacity and laser thermal shock tests by the IF method.

Table 2.1.1. Conditions for Synthesizing FGM/NFGM

Temperature		1300-1500°C
Pressure		10-100 Torr
Material gas	CH_4	80-600 cc/min
	$SiCl_4$	0-200 cc/min
	H_2	0-600 cc/min
Substrate (graphite)		50 mm x 50 mm

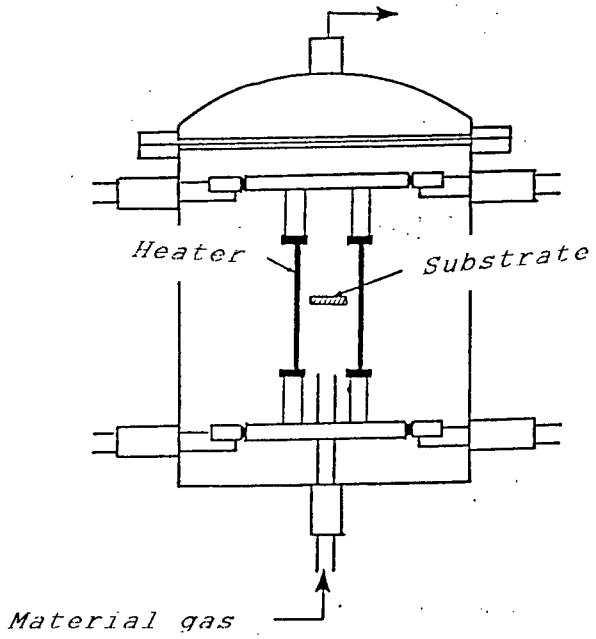

Figure 2.1.1. CVD equipment of hot-wall type

(2) Thermal properties: The coefficient of thermal expansion was measured by the laser interference method (LIX-1 made by Shinku Rikoh, Ltd.) within the limits from the room temperature to 600°C. In addition, the coefficient of thermal expansion was measured by the laser flash method (TC-7000 made by Shinku Rikoh), and the specific heat capacity by the DSC method (DSC200 made by Seiko Electronic Industry, Ltd.). Thus the thermal conductivity was calculated from the products of the coefficient of thermal expansion, specific heat and density. We requested Shizuoka University to evaluate data for the measurement of thermal properties.

(3) Microscopic structural analysis and crystal structure: These items were dealt with by means of SEM and laser Raman.

3. Principal Results

3.1. Study of Scaling Up

On the basis of the results of basic research by the Hirai Laboratory, we investigated the NFGM synthesis of the C/SiC system through the $CH_4+SiCl_4+H_2$ system and the $C_3H_8+SiCl_4+H_2$ system. With a view to uniformly producing plate-shaped films, we studied intra-furnace geometry in addition to such synthesis conditions as temperature, pressure and gas composition and flow. As a result, we found it possible to synthesize an NFGM with the size of 35 mm x 35 mm x 2 mm, above the 30ϕ that is the target for the first term, by the $CH_4+SiCl_4+H_2$ system, within the limits of C/(SiC+C) = 0-100mol%. Figure 3.1.1 shows the relationship between the ratio of material gas mixture and the NFGM composition.

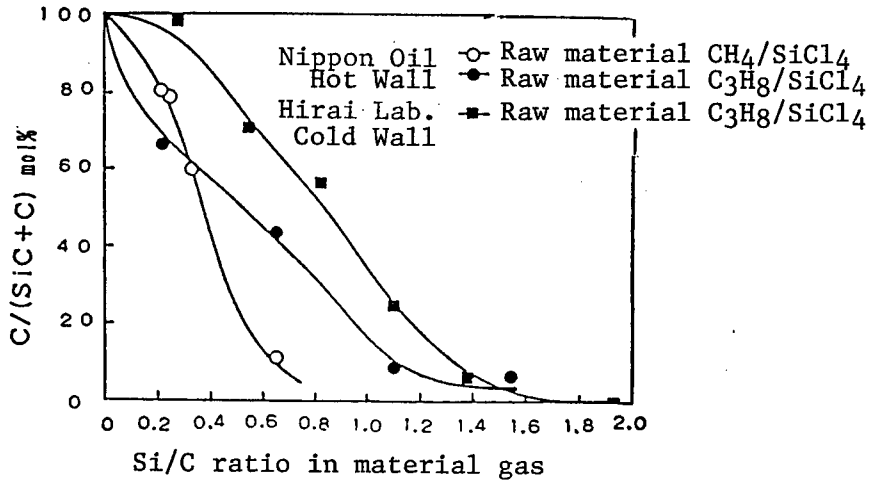

Figure 3.1.1. Relationship between the ratio of material gas mixture and NFGM composition

3.2. Production of NFGM and Evaluation of Its Properties

(1) Mechanical properties: We synthesized NFGM's of various compositions and furnished about 100 test pieces of various kinds to the properties evaluation group. A representative photo of a synthesized NFGM and test pieces clipped out is given in Figure 3.2.1. Figure 3.2.2 shows the result of MST test of NFGM's conducted by the materials strength research facility of Tohoku University. It was found impossible for the mechanical properties of an NFGM, intermediately composed between C and SiC, to be readjusted by the rule of simple mixture.

(2) Thermal properties: The result of measuring the average thermal expansion coefficient of NFGM's is given in Figure 3.2.3. The coefficient of thermal expansion is in close agreement with that of an NFGM synthesized by the cold-wall method, and the coefficient does not become very low even in a composition close to C = 90mol%. The NFGM thermal conductivity calculated from the rate of thermal diffusion and the specific heat capacitance is shown in Figure 3.2.4.

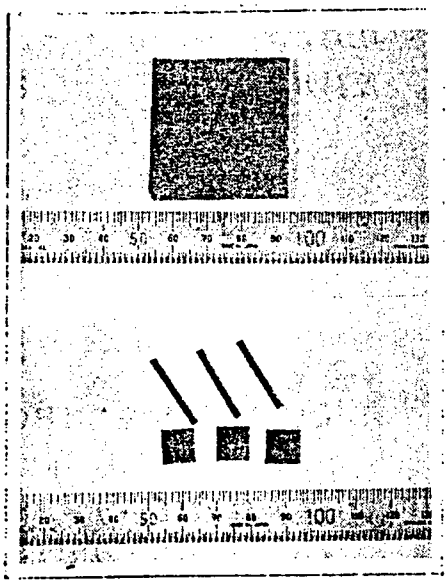

Figure 3.2.1. Synthesized NFGM
(Up) after synthesis
(Down) MSP and bending test pieces

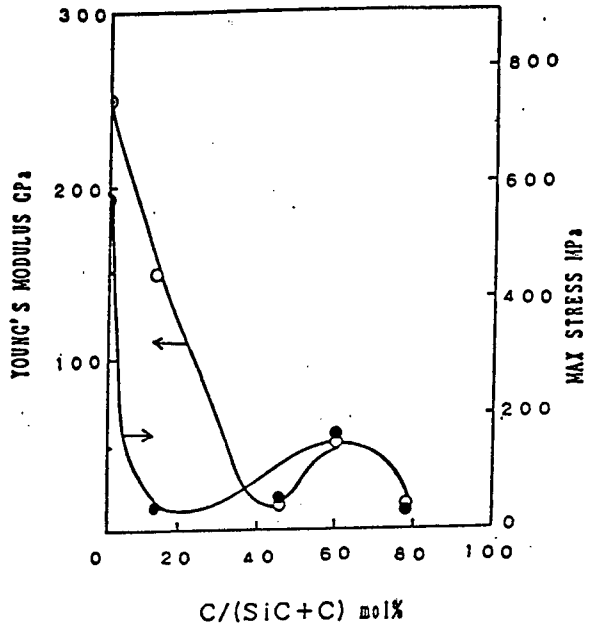

Figure 3.2.2. Composition of NFGM and its mechanical properties (MSP test)

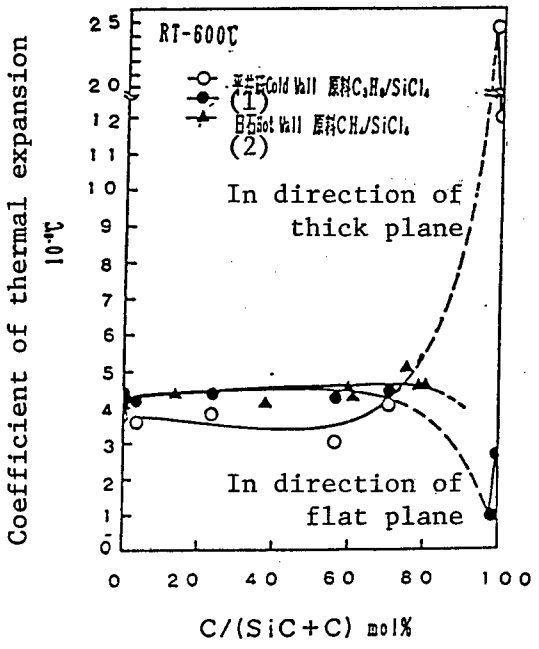

Figure 3.2.3. Composition and thermal expansion coefficient of NFGM

Key:
1. Hirai Lab. Cold wall Raw material $C_3H_8/SiCl_4$
2. Nippon Oil Hot wall Raw material $CH_4/SiCl_4$

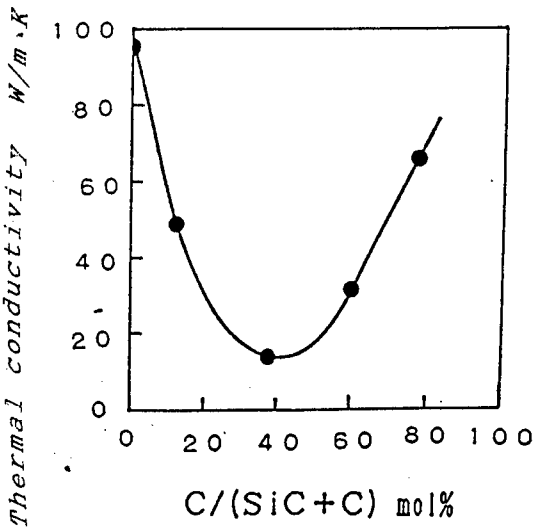

Figure 3.2.4.

(3) Fine structure of NFGM's and its properties: The fractures after MSP tests are shown in Figure 3.2.5 [not reproduced]. It was found that in the vicinities of C = 15mol% and C = 80mol%, the structure is comparatively porous, and that the structure changes with a change in composition.

The size of carbon crystallites in NFGM's was measured by laser Raman. Figure 3.2.6 shows the relationship between the NFGM composition and the size of carbon crystallites in NFGM's. These results revealed that in the case of C/SiC materials produced by CVD, there are changes not only in chemical composition but also in macroscopic structures with porosity, etc., and in microscopic structures with crystallinity.

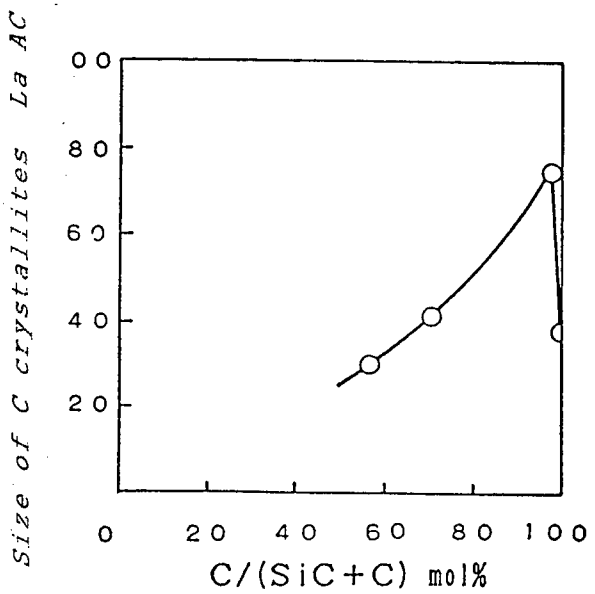

Figure 3.2.6. NFGM composition and the size of C crystallites (measured with laser Raman spectrometer)

3.3. FGM Coating on C/C Composites

(1) Production of a step FGM: We trial-manufactured a C/SiC→SiC six-step FGM on a graphite substrate. The result of this trial-manufacture is shown in Figure 3.3.1. From a SEM image and the result of EMPA analysis, we found that a step FGM with a size of 35 mm x 35 mm x 2 mm had been created.

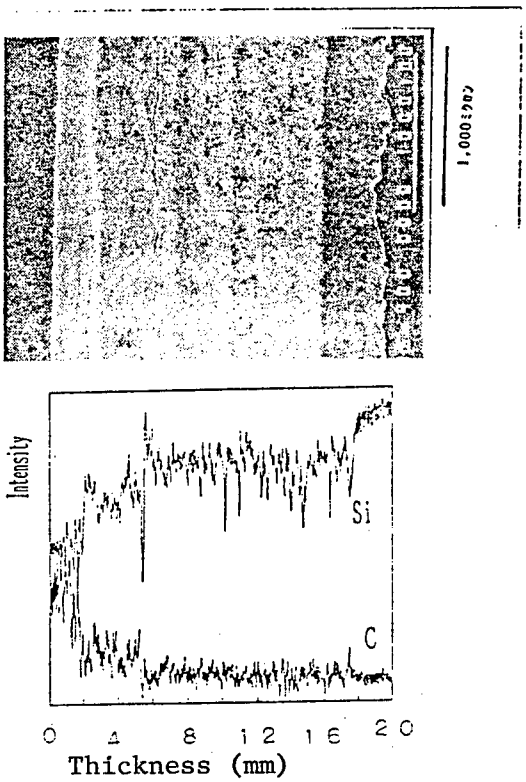

Figure 3.3.1. SEM image of step FGM

(2) Measures to cope with complex forms: Prior to the FGM coating on C/C composites, we synthesized a C/SiC→SiC FGM on a graphite substrate material of a cylindrical type (outer diameter: 21 mm; inside diameter: 15 mm). The result is shown in Figure 3.3.2. These can be thought to suggest the possibility of coating on materials in complex forms for future C/C composites.

3.4. CVI+FGM

(1) We are considering CVI (chemical vapor infiltration) + FGM as a method to form FGM's from inside C/C composites. 3D fabrics consisting of highly elastic pitch carbon fiber are shown in Figure 3.4.1, and their internal structure is given in Figure 3.4.2. When we infiltrated SiC or C/SiC into 3D fabrics consisting of carbon fiber by the CVI method, we found a difference between SiC and C/SiC in the way cracking occurred. Therefore, it is conceivable that ceramic composite materials reinforced in many directions can be produced by means of CVI+FGM.

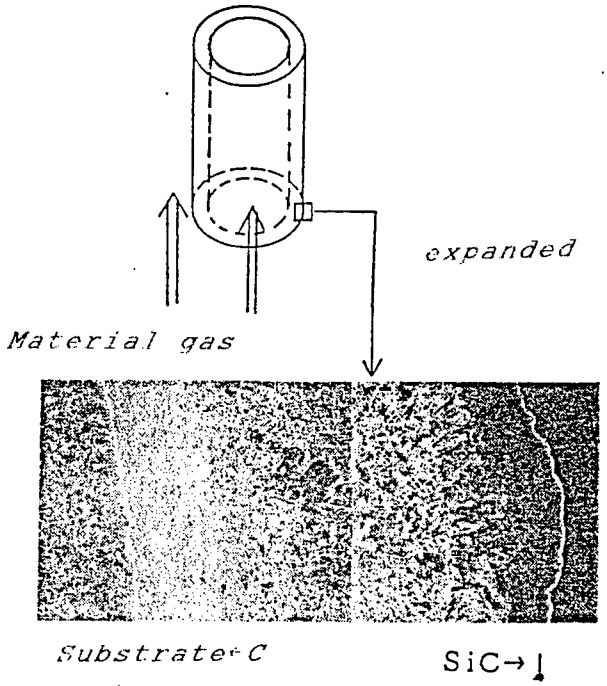

Figure 3.3.2. FGM synthesized on cylindrical graphite substrate material

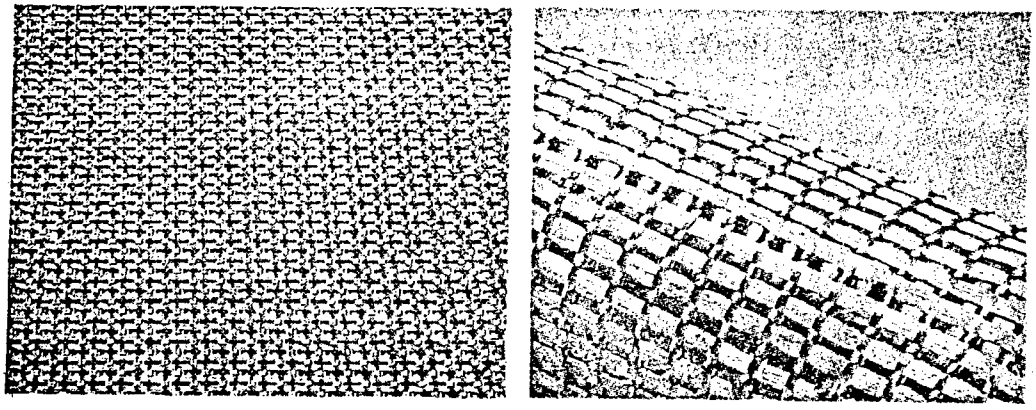

Figure 3.4.1. 3D fabrics of pitch carbon fiber (panels and cylinders)

(2) On the supposition of CVI+FGM using three-dimensional fabrics of carbon fiber, we formed a C/SiC→SiC six-step FGM on carbon fiber. A microscopic photo of this product is given in Figure 3.4.3. Generally uniform films were formed for forms other than those of flat plates, with the characteristics of the CVD method utilized.

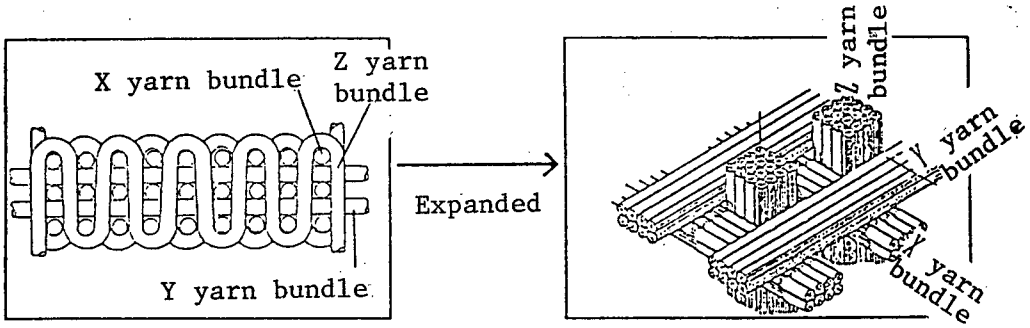

Figure 3.4.2. Structure of 3D fabrics of carbon fiber

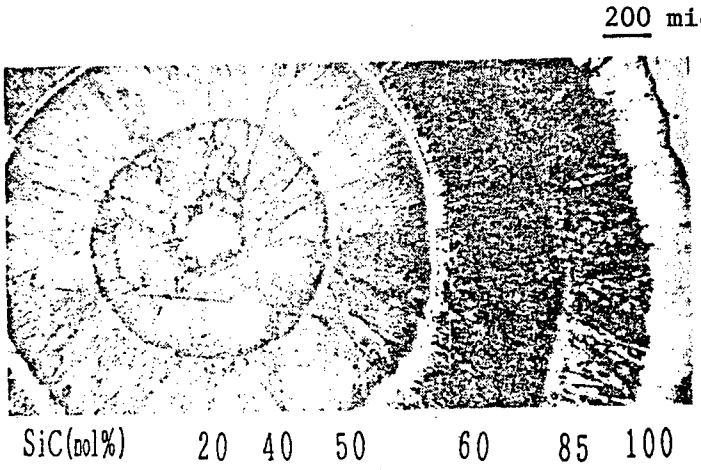

Figure 3.4.3. Six-step FGM formed on carbon fiber

4. Conclusion

We conducted studies on the scaling up of FGM's for the purpose of producing evaluation-oriented NFGM's for materials design and responding to the requirement for larger FGM's for the future. We have thus established techniques to produce 35 mm x 35 mm FGM's by the CVD method. In addition, we have prospects for FGM synthesis on materials of complex forms and on carbon fibers, as our preliminary studies on coating for C/C composites and on CVI+FGM. We are scheduled to continue our efforts to optimize manufacturing conditions and our approaches to future themes.

Production of TiC-Ti and C-SiC Functionally Gradient Materials Using C/C Composite as Basic Material

43067008H Tokyo FGM 89 in Japanese 14 Sep 89 pp 79-82

[Report by Chihiro Kawai and Ren Igarashi of Sumitomo Electric Industries, Ltd.]

[Text] 1. Introduction

Carbon fiber reinforced carbon composite materials (C/C composites) exhibit superior specific strength and specific rigidity even at high temperatures above 1000°C. Therefore, expectations have recently been placed on their use in the future as materials for aeronautical and space purposes, such as space shuttles. On the other hand, C/C composites have two big defects.

The first defect is that they are not very resistive to oxidation. The effective way to improve their oxidation resistance is to coat them with ceramics consisting of SiC, Si_3N_4, etc. However, when they are directly coated by such methods as CVD, a difference between the two in the coefficient of thermal expansion brings about thermal cracks due to the tensile stress arising in ceramic layers when they are cooled to room temperature after the coating. For this reason, the oxidation resistance declines markedly, because the thermal expansion coefficient of C/C composites is extremely low.

The second defect is that it is difficult to combine a C/C composite and a metal. With regard to a junction layer to be formed on a C/C composite, it is desirable that it be strongly adhesive and that the surface of the junction layer be metallic. Currently, directly metallized layers, plated layers, welded layers, etc., are used for this purpose, but they do not provide any satisfactory adhesion.

In this research, which is designed for oxidation resisting coating on C/C composites, we carried out C-SiC system gradient composition coating by the CVD method for the purpose of easing the thermal stress that occurs in coating layers and providing them with superior resistivity to oxidation, and also carried out TiC-Ti system gradient composition coating by the PVD method for the purpose of forming junction layers consisting of C/C composites and metals, and thus evaluated their properties.

2. Methods of Experiments

2-1. C-SiC System (CVD)

As a material gas we used a mixture of $SiCl_4$, CH_4, and H_2. The thermal dynamic equilibrium precipitation phases in these systems at the reaction temperatures of 1300-1500°C and the pressure of 20-100 torr were calculated by computers. On the basis of these calculations we carried out experiments changing the composition of raw materials in various ways, and thus evaluated the composition of deposit layers, precipitation speed, structures, etc. Next, we continuously changed the composition of the material gas with the lapse of coating time on the basis of the basic data obtained, using the C/C composite as the basic material, thereby coating the C-SiC system gradient composite layers by 0.5-2 mm, and observed such things as the structure of the coating layers and how thermal cracks occurred in the SiC layer on the uppermost surface.

2-2. TiC-Ti System (PVD)

We melted and evaporated Ti by the use of HCD-type ion plating equipment, caused it to react with introduced CH_4 gas, and formed TiC-Ti composite layers of 20-30 μm size on a C/C composite substrate previously kept at room temperature~900°C. We controlled the composition by changing the flow of the CH_4 gas to be introduced and, in the case of gradient composition coating, we continuously changed the CH_4 flow with the lapse of coating time. We heated the produced samples in a vacuum for 1 hour within the limits of 700-1350°C, identified the phase change in the coating layers before and after the heating by means of X-ray diffraction and EMPA analysis, and examined the thermal stability of the composition of the coating layers. In addition, we measured the change in the adhesion of the coating layers before and after the heating by the scratch method.

3. Results and Consideration

3-1. Production of C-SiC Functionally Gradient Materials

Figure 3.1.1 shows the thermodynamic equilibrium precipitation phases of the three component systems--$SiCl_4$, CH_4 and H_2--at 1400°C and 60 Torr. As a result of experiments in the component lines shown in Figure 1, we found it possible to carry out C-SiC system coating by changing the compositions of $SiCl_4$ and CH_4 in the material gas on line A.

Figure 3.1.2 shows the relationship between the Si/Cmol% in the material gas and the composition in the deposit layer. Compared with the thermodynamic equilibrium composition, the composition of the coating layer is rich in SiC.

Figure 3.1.3 shows the precipitation speed of the C-SiC system composite layer of each composition. The total precipitation speed dropped with an increase in the C content in the deposition layer.

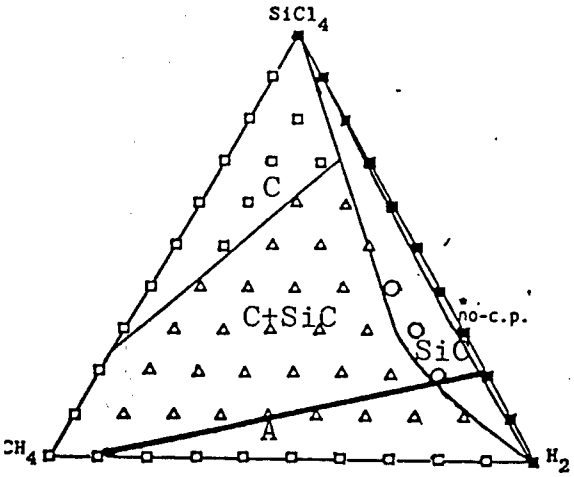

Figure 3.1.1. Equilibrium precipitation phases of $SiCl_4$-CH_4-H_2 systems (1400°C, 60 Torr)

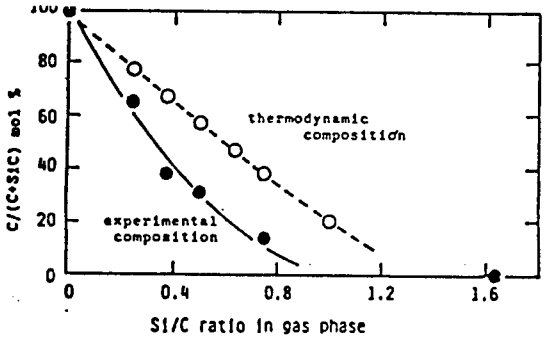

Figure 3.1.2. Relationship between the composition of material gas and deposition layer

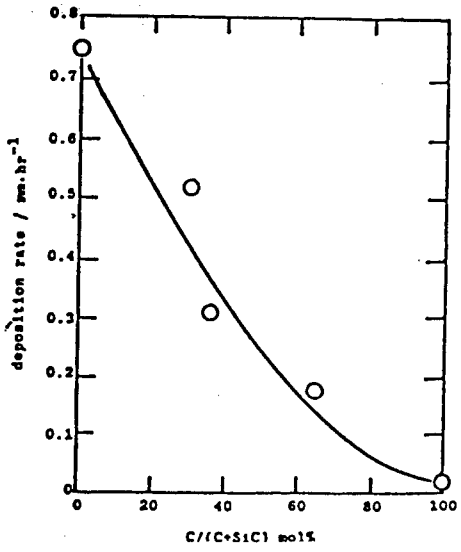

Figure 3.1.3. Relationship between the composition of deposition layer and precipitation speed

This is conceivably due to the fact that the precipitation speed of C is lower than that of SiC.

Figure 3.1.4 shows sectional optical microscopic photos of the C-SiC composite phases of various compositions. The structure becomes porous with an increase in C content. The SiC in the composite phases grows in the form of fiber, all showing a (220) orientation regardless of composition.

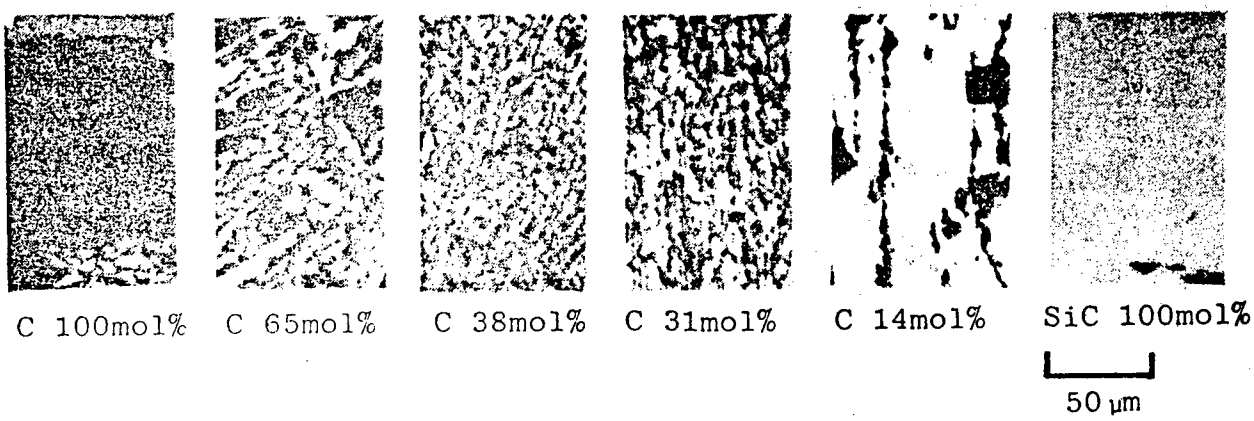

Figure 3.1.4. Structures of C-SiC system composite phases of various compositions (optical microscopic images)

A sectional optical microscopic photo of a C-SiC system gradient composition layer for which a C/C composite is coated is shown in Figure 3.1.5, and a SEM image of the SiC in the upper layer is given in Figure 3.1.6. Coating the C/C composite with the C-SiC system gradient composition layer caused the number of thermal cracks arising in the SiC layer on the upper surface to decrease remarkably compared with SiC coating. However, in view of the fact that there are some thermal cracks caused on the coating layer, the function of gradient composition to ease thermal stress is not sufficient. It is necessary to study ways to make the composition gradient from within the basic material.

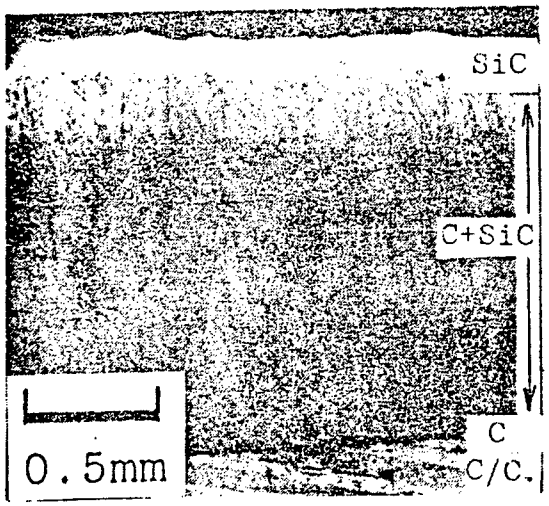

Figure 3.1.5. Sectional structure of C-SiC system gradient composition layer with which a C/C composite is coated (optical microscopic image)

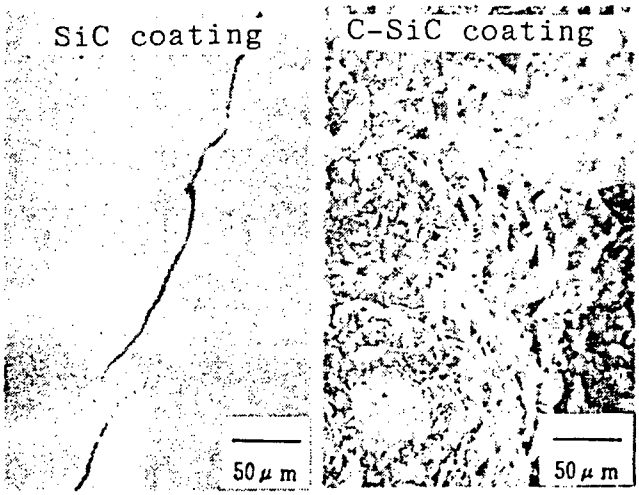

Figure 3.1.6. Surface SiC structure of C-SiC system gradient composition layer (SEM image)

3-2. Production of TiC-Ti System Functionally Gradient Materials

We chose Ti as a metallic layer to be used for junction, and TiC as a layer to closely adhere to carbon materials. However, since the speed of C diffusion in a metal Ti in a high temperature is very high, it is conceivable that Ti will change into TiC due to the C diffusion arising from C's density gradient, when the temperature rises to a degree needed for the junction, in the case of the coating layer being made to consist of TiC/Ti two layers. In this research, therefore, we produced a structure to restrain the C diffusion in the coating layer to a minimum level by making the composition between Ti and TiC gradient in order to minimize the density gradient of the C in the coating layer.

Figure 3.2.1 is an X-ray diffraction diagram showing the flow and deposit phase of CH_4 gas to react with Ti steam in HCD-type ion plating equipment. By controlling the CH_4 flow we obtained Ti-TiC system composite phases of various compositions. On the basis of this result, we coated the C/C composite with a TiC-Ti system gradient composition layer by continuously changing the CH_4 flow with the lapse of coating time.

Figure 3.2.2 shows a sectional optical microscopic image of a TiC-Ti system gradient composition layer and EPMA density distribution.

Figure 3.2.3 shows the adhesive strength of the coating layer and its phase change before and after heating a TiC-Ti system functionally gradient material, formed on a C/C composite basic material, at various temperatures for 1 hour.

Figure 3.2.4 shows an EPMA composition analysis of the cross section of the coating layer when heated at 1000°C for 1 hour.

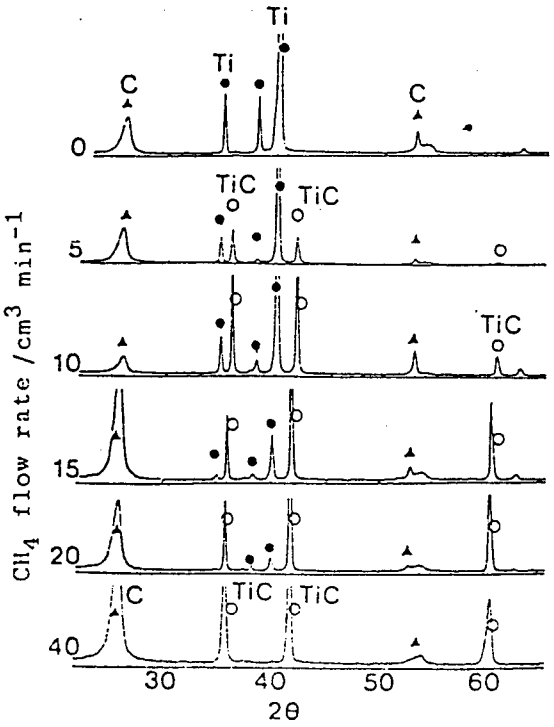

Figure 3.2.1. Relationship between CH_4 flow and deposit phase in TiC-Ti system coating

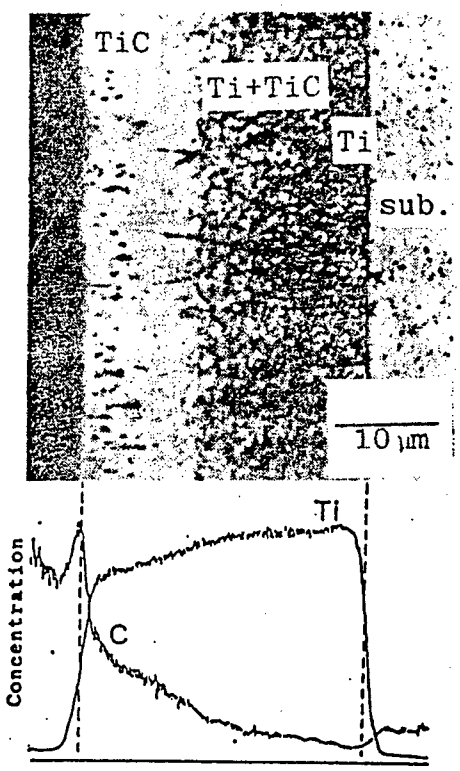

Figure 3.2.2. Sectional structure of TiC-Ti system gradient composition layer (optical microscopic image after chemical etching)

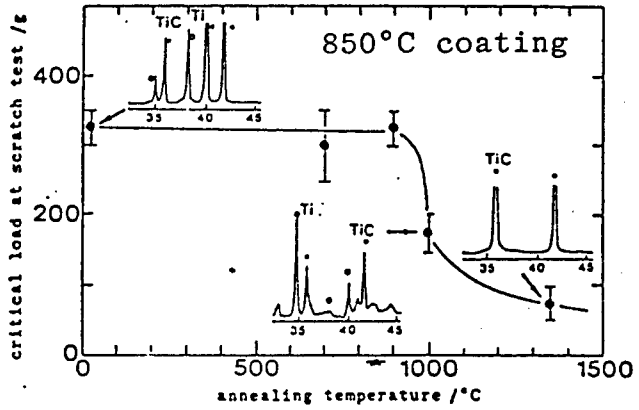

Figure 3.2.3. Relationship between the adhesive strength and phase change of the coating layer through heating TiC-Ti system gradient composition layer with which C/C composite is coated

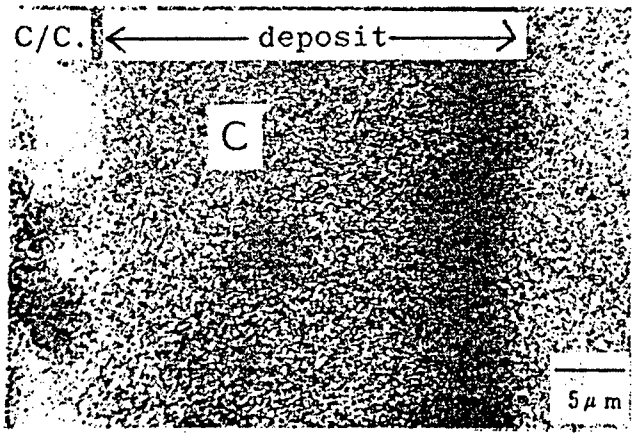

Figure 3.2.4. Distribution of C atom density in the cross section of the coating layer after it is heated at 1000°C for 1 hour

We found that a high degree of adhesion can be preserved up to the heating temperature of 900°C by fixing the coating temperature at 850°C. In addition, we discovered that the Ti layer on the surface of the coating layer is stable even when it is heated at 1000°C for 1 hour, by holding down the C diffusion from the substrate material and that in the coated layer to a minimum level.

This research was carried out as part of the "Studies on Basic Techniques for the Development of Functionally Gradient Materials To Reduce Thermal Stress," conducted in the fiscal 1988 expenditure for the promotion and coordination of science and technology.

- END -

10

22161
45

NTIS
ATTN: PROCESS 103
5285 PORT ROYAL RD
SPRINGFIELD, VA 22161

Foreign Broadcast Information Service (FBIS) and Joint Publications Research Service (JPRS) publications contain political, economic, military, and sociological news, commentary, and other information, as well as scientific and technical data and reports. All information has been obtained from foreign radio and television broadcasts, news agency transmissions, newspapers, books, and periodicals. Items generally are processed from the first or best available source; it should not be inferred that they have been disseminated only in the medium, in the language, or to the area indicated. Items from foreign language sources are translated; those from English-language sources are transcribed, with personal and place names rendered in accordance with FBIS transliteration style.

Headlines, editorial reports, and material enclosed in brackets [ ] are supplied by FBIS/JPRS. Processing indicators such as [Text] or [Excerpts] in the first line of each item indicate how the information was processed from the original. Unfamiliar names rendered phonetically are enclosed in parentheses. Words or names preceded by a question mark and enclosed in parentheses were not clear from the original source but have been supplied as appropriate to the context. Other unattributed parenthetical notes within the body of an item originate with the source. Times within items are as given by the source. Passages in boldface or italics are as published.

SUBSCRIPTION/PROCUREMENT INFORMATION

The FBIS DAILY REPORT contains current news and information and is published Monday through Friday in eight volumes: China, East Europe, Soviet Union, East Asia, Near East & South Asia, Sub-Saharan Africa, Latin America, and West Europe. Supplements to the DAILY REPORTs may also be available periodically and will be distributed to regular DAILY REPORT subscribers. JPRS publications, which include approximately 50 regional, worldwide, and topical reports, generally contain less time-sensitive information and are published periodically.

Current DAILY REPORTs and JPRS publications are listed in *Government Reports Announcements* issued semimonthly by the National Technical Information Service (NTIS), 5285 Port Royal Road, Springfield, Virginia 22161 and the *Monthly Catalog of U.S. Government Publications* issued by the Superintendent of Documents, U.S. Government Printing Office, Washington, D.C. 20402.

The public may subscribe to either hardcover or microfiche versions of the DAILY REPORTs and JPRS publications through NTIS at the above address or by calling (703) 487-4630. Subscription rates will be provided by NTIS upon request. Subscriptions are available outside the United States from NTIS or appointed foreign dealers. New subscribers should expect a 30-day delay in receipt of the first issue.

U.S. Government offices may obtain subscriptions to the DAILY REPORTs or JPRS publications (hardcover or microfiche) at no charge through their sponsoring organizations. For additional information or assistance, call FBIS, (202) 338-6735,or write to P.O. Box 2604, Washington, D.C. 20013. Department of Defense consumers are required to submit requests through appropriate command validation channels to DIA, RTS-2C, Washington, D.C. 20301. (Telephone: (202) 373-3771, Autovon: 243-3771.)

Back issues or single copies of the DAILY REPORTs and JPRS publications are not available. Both the DAILY REPORTs and the JPRS publications are on file for public reference at the Library of Congress and at many Federal Depository Libraries. Reference copies may also be seen at many public and university libraries throughout the United States.